# Geochemical Profiles Across the Listvenite-Metamorphic Transition in the Basal Megathrust of the Semail Ophiolite: Results from Drilling at Oman DP Hole BT1B

**M. Godard[1*], E. Carter[2], T. Decrausaz[1], R. Lafay[1], E. Bennett[3], F. Kourim[4], J.-C. de Obeso[5], K. Michibayashi[6], M. Harris[7], J. Coggon[8], D. Teagle[8], P. Kelemen[5] and the Oman Drilling Project Phase 1 Science Party†**

[1] Géosciences Montpellier, CNRS, Université de Montpellier, Montpellier, France

[2] Department of Earth and Environmental Sciences, The University of Manchester, Manchester, United Kingdom
Now at: Department of Geology, Trinity College Dublin, Dublin 2, Ireland

[3] School of Earth and Ocean Sciences, Cardiff University, Cardiff, United Kingdom

[4] Academia Sinica, Institute of Earth Science, Taipei, Taiwan

[5] LDEO, Columbia University, Palisades, NY, United States

[6] Dep. Earth and Planetary Sciences, Graduate School of Environmental Studies, Nagoya University, Nagoya, Japan

[7] School of Geography, Earth and Environmental Sciences, Plymouth University, Plymouth, United Kingdom

[8] School of Ocean & Earth Science, University of Southampton, United Kingdom

* Corresponding author: Marguerite Godard (Marguerite.Godard@umontpellier.fr)

**Key Points:**

- Listvenitization induce a mass increase of up to 51% (50 % volume) relative to the serpentinized mantle protolith
- FME distribution suggests reactions with several batches of $CO_2$-rich fluids over various flow paths parallel to the basal thrust
- Listvenitization could represent a major trap-and-release mechanism for water and FME as well as $CO_2$ along convergent margins

## Abstract

The transition from the Semail ophiolite mantle to the underlying metamorphic sole was drilled at ICDP OmanDP Hole BT1B. We analyzed the bulk major, volatile and trace element compositions of the mantle-derived listvenite series and metamorphic rocks, with the aim to constrain chemical transfers associated to peridotite carbonation along the ophiolite basal thrust. The listvenite series comprise variously carbonated serpentinites and (fuchsite-bearing) listvenites. They have high $CO_2$ (up to 43.2 wt.%) and variable $H_2O$ (0-12.1 wt.%). Yet, they have compositions close to that of the basal banded peridotites for most major and lithophile trace elements, with fuchsite-bearing listvenites overlapping in composition with amphibole-bearing basal lherzolites (e.g., $Al_2O_3$= 0.1-2.2 wt.%; Yb= 0.05-1 x CI-chondrite), The protolith of the listvenite series was likely similar in structure and composition to serpentinized banded peridotites which immediately overlie the metamorphic sole elsewhere in Oman. The listvenite series are enriched in fluid mobile elements (FME) compared to Semail peridotites (up to ~$10^3$-$10^4$ x Primitive Mantle), with concentrations similar to the underthrusted metabasalts and/or metasediments for Cs, Sr and Ca and sometimes even higher for Pb, Li, As, and Sb (e.g., Li up to 130 ppm; As up to 170 ppm). We also observe a decoupling between Sr-Ca enrichments and other FME, indicating interactions with several batches of deep $CO_2$-rich fluids transported along the basal thrust. These results suggest that peridotite carbonation could represent one of the major trap-and-release mechanisms for carbon, water and FME along convergent margins.



## Plain Language Summary

Ophiolites are sections of oceanic lithosphere emplaced on land as plates converge. The faults developed at their base are analogues to plate interfaces in subduction zones, where mass transfers occur and play a key role in the global cycling of elements. A core was drilled at the base of the Semail Ophiolite, where variously hydrated and carbonated mantle rocks known as serpentinites and listvenites witnessed major fluid fluxes. Reactions with $CO_2$-bearing fluids (carbonation reaction) enhanced the mobility of elements during mass transfers along the basal thrust. We measured the chemistry of 84 samples spaced along this core. Results indicate that $CO_2$-bearing fluids derive from at least two sources or pathways. As peridotites reacted, their volume increased, causing cracking, enhancing the ingress of reactive fluids and participating to (almost) complete carbonation of the basal ophiolite mantle. Carbon as well as many elements such as cesium, arsenic, antimony, lead became enriched in these rocks. If forming in subduction zones, listvenites may act as temporary storage for these elements and impact global chemical cycles.


**Keyword :** Peridotites, Serpentinization, Carbonation, Si-metasomatism, Fluid-rock interactions, Mass balance, geochemical cycles, Fluid pathways, ICDP Oman Drilling Project

## 1 Introduction

Listvenites (or listwaenites) are produced by $CO_2$-metasomatism of mantle-derived ultramafic rocks [*Falk and Kelemen*, 2015; *Halls and Zhao*, 1995]. They are composed mainly of quartz and carbonate (magnesite and/or dolomite, ± Cr- or Mg-rich micas ± chlorite) and are often associated with serpentinites, ophicarbonates and/or talc. Since their first description in the literature [*Rose*, 1837], they have been investigated for one of their main characteristics: the occurrence of mineralizations concentrating economically-valuable metals, such as Au, Pb-Hg-Ag, Cu, Ni, Co or Sb (e.g., [*Belogub et al.*, 2017; *Buisson and Leblanc*, 1985; *Escayola et al.*, 2009; *Halls and Zhao*, 1995; *Laznicka*, 2010]). More recently, they have been studied also as natural analogues for industrial geological carbon storage in ultramafic basement [*Falk and Kelemen*, 2015; *Hansen et al.*, 2005; *Ulrich et al.*, 2014]. These studies have highlighted the structural, mineralogical and petrological complexity of listvenites, thus resulting in a wealth of different and sometimes contradictory genetic models [*Belogub et al.*, 2017; *Falk and Kelemen*, 2015; *Halls and Zhao*, 1995; *Nasir et al.*, 2007]. Some authors invoke serpentinization of mantle peridotites followed by the formation, concurrent or consecutive, of carbonate (carbonation) and quartz (silicification) [*Boschi et al.*, 2009; *Nasir et al.*, 2007; *Stanger*, 1985; *Ulrich et al.*, 2014], whilst some emphasize direct reactions with primary mantle minerals [*Hansen et al.*, 2005; *Kelemen et al.*, 2011; *Power et al.*, 2013]. Other authors stress the role of the composition of the infiltrating $CO_2$-bearing fluid rather than that of the protolith in the genesis of listvenites and associated ore-grade mineralizations [*Belogub et al.*, 2017; *Escayola et al.*, 2009; *Halls and Zhao*, 1995; *Menzel et al.*, 2020a; *Menzel et al.*, 2018; *Stanger*, 1985], often emphasizing a possible imprint of silica and other cations scavenged from neighboring lithologies [*Nasir et al.*, 2007; *Ulrich et al.*, 2014].

The estimated temperatures of formation and the proposed source(s) of fluids also differ: fluid-inclusions and thermodynamic analyses of carbonate-quartz assemblages suggest reaction within a temperature range of 120-280°C (down to 80°C and up to 400°C) and likely triggered by the infiltration of slab-derived fluids [*Belogub et al.*, 2017; *Boskabadi et al.*, 2020; *Escayola et al.*, 2009; *Hansen et al.*, 2005; *Menzel et al.*, 2018]. However, petrographic and geochemical analyses show also that some listvenite series were formed during weathering (<50°C) by silicification reactions triggered by interactions with fluids in equilibrium with atmospheric $CO_2$ (e.g., [*Stanger*, 1985; *Ulrich et al.*, 2014]) whilst other others show evidence for distinct fluid infiltration and weathering episodes (e.g., [*Nasir et al.*, 2007]). Finally, the mechanisms allowing the infiltration of the $CO_2$-rich metasomatic fluids remain speculative with suggested mechanisms including the role of large faults and deformation, reactive cracking and dissolution [*Escayola et al.*, 2009; *Falk and Kelemen*, 2015; *Nasir et al.*, 2007]. The first difficulty to unravel the genesis of listvenites stems from their environments: they outcrop along ophiolitic and orogenic belts as part of highly altered rock assemblages, which often have undergone several stages of metamorphism (e.g., [*Azer et al.*, 2019; *Halls and Zhao*, 1995; *Menzel et al.*, 2018; *Nasir et al.*, 2007]). For these reasons, both the protolith and potential $CO_2$ source(s) for listvenite-forming metasomatism are highly metamorphosed and difficult to identify, and display a large structural and compositional variability. Only a few sites allow sampling the transition from mantle peridotites to the possible source(s) of $CO_2$ metasomatism: the Semail ophiolite is one of them.

The Semail ophiolite is a fragment of Tethyan oceanic lithosphere tectonically emplaced on the Arabian plate at the end of the Cretaceous (Fig. 1a). Listvenite bodies occasionally crop

out along its basal thrust ([*Falk and Kelemen*, 2015; *Glennie et al.*, 1974; *Nasir et al.*, 2007]; Fig. 1a). In 2017, a 300m long section was drilled through one of the largest bodies, north of Wadi Mansah (Fanjah, Sultanate of Oman; Fig 1a), as part of the ICDP Oman Drilling Project (OmanDP, [*Kelemen et al.*, 2020b]). OmanDP Hole BT1B sampled the transition from listvenites at the base of the ophiolite to the metamorphic sole: ~200 m of listvenites and variously carbonated serpentinites overlapping ~100m of greenshists and greenstones were recovered (Fig. 1b). This sampling allows us to quantify the broad and complex range of mineralogy and rock types that are typical of listvenite suites and, for the first time, to correlate these variations to the distance to their possible source(s). In particular, the basal thrust, which intersects the core at 200 m depth, is considered as one of the major pathways for fluids triggering the formation of listvenites, and neighboring lithologies [*Falk and Kelemen*, 2015; *Nasir et al.*, 2007].

We carried out a bulk rock geochemical study (major, volatile and trace elements) of 84 samples representative of the different lithologies recovered at OmanDP Hole BT1B. Our results allow enable us to document the bulk composition of these different lithologies and their downhole mineralogical and geochemical variations from the sample scale to that of the borehole. This provides important new insights into the composition of the protolith of the Semail listvenite series and of the underlying metamorphic lithologies, and highlights the magnitude of fluid-mediated elemental transfers associated to the formation of listvenites along the basal thrust and into the overlying ophiolitic mantle. It is suggested that such mass fluxes may represent an important trap-release mechanism for fluid mobile elements in global geochemical cycles.

## 2 Geological Setting

### 2.1 The Semail Ophiolite

The Semail ophiolite, composed of a dozen structural massifs outcropping over 500 km along the north-eastern margin of the Arabian Plate (~20000 km$^2$), is regarded as one of the world's largest and best documented ophiolites (Fig 1a, [*F Boudier and Nicolas*, 1988; *Coleman and Hopson*, 1981; *Goodenough et al.*, 2010; *Lippard et al.*, 1986; *Peters et al.*, 1991; *Searle*, 2019]). The 5-7 km thick structural massifs expose continuous fragments of the Tethyan oceanic lithosphere that were initially more than 12-15 km thick according to structural reconstitutions [*Lippard et al.*, 1986; *Nicolas et al.*, 2000] suggesting tectonic erosion during emplacement and/or post obduction. The ophiolitic sequence comprises a thick mantle section overlain by a well preserved layered oceanic crust, from lower gabbros to upper volcanics [*Lippard et al.*, 1986; *Nicolas et al.*, 2000], formed at the end of the Cretaceous (96.12–95.50 Ma [*Rioux et al.*, 2012; *Rioux et al.*, 2016]). The geochemistry of the upper volcanics indicates a transition from oceanic accretion to subduction related volcanism (e.g., [*Belgrano et al.*, 2019; *Ernewein et al.*, 1988; *Godard et al.*, 2003]), that has been interpreted as evidence for a spontaneously initiating subduction (e.g., [*MacLeod et al.*, 2013; *Pearce et al.*, 1981]), or a change in geodynamic settings, from mid-ocean ridge to intra-oceanic underthrusting and, possibly, incipient subduction (e.g., [*Boudier et al.*, 1988; *Godard et al.*, 2006; *Goodenough et al.*, 2010]).

The mantle section is predominantly made up of moderately serpentinized (40-80 %) depleted harzburgites with minor dunites [*Boudier et al.*, 2010; *Godard et al.*, 2000; *Hanghoj et al.*, 2010; *Hopson et al.*, 1981], that preserve the microstructural fabric of asthenospheric deformation below the oceanic spreading center [*Boudier and Coleman*, 1981]. Low temperature

ductile deformation overprints this early deformation towards the base of the mantle section and has been ascribed to the onset of the ophiolite detachment (e.g., [*Boudier et al.*, 1988; *Linckens et al.*, 2011; *Nicolas et al.*, 2000]). Local occurrences of lherzolites (>5 % clinopyroxene, Cpx) and Cpx-harzburgites (>2 % Cpx) are also described in this lowermost mantle section, generally in massifs where the thickest mantle sections were preserved (e.g. Fizh [*Takazawa et al.*, 2003]; Wadi Tayin [*Godard et al.*, 2000; *Hanghoj et al.*, 2010]) and/or close to areas where the ophiolitic metamorphic sole outcrops [*Khedr et al.*, 2014]. These Cpx-rich basal peridotites have been interpreted as the result of variable melt extraction along the palaeoridge [*Khedr et al.*, 2014; *Le Mée et al.*, 2004; *Monnier et al.*, 2006] or, alternatively, as due to refertilization reactions at the base of the oceanic mantle lithosphere during off-axis cooling or early intraoceanic thrusting [*Godard et al.*, 2000; *Lippard et al.*, 1986; *Takazawa et al.*, 2003].

The ophiolite lies upon a series of underthrusted sheets of pelagic and turbiditic sediments, shelf carbonates, as well as volcanics, mainly of alkaline composition (sometimes referred to as Haybi volcanics) with minor transitional to tholeiitic components [*Bechennec et al.*, 1990; *Chauvet et al.*, 2011; *Lippard et al.*, 1986; *Maury et al.*, 2003]. These lithologies commonly grouped as the Hawasina assemblages are the relicts of a wide oceanic basin (at least 540 km large), that formed during the breakup and thinning of the Arabian continental margin during Permian to Trias [*Bechennec et al.*, 1990].

The ophiolite *sensu stricto* and the underlying allochtonous units were thrusted atop the Arabian platform during late Cretaceous (e.g., [*Glennie et al.*, 1974; *Searle and Malpas*, 1980]). Slivers of the ophiolite metamorphic sole are preserved at the transition from the allochtonous units to the base of the ophiolite mantle section. They are locally overlain by <200m thick (proto-)mylonitic "banded lherzolites", deformed parallel to the basal contact, comprising alternating highly serpentinized lherzolites (or Cpx-harzburgites) and olivine rich harzburgites and dunites [*Lippard et al.*, 1986; *Prigent et al*, 2018a]. These commonly preserve evidence of secondary amphibole formed at the expense of Cpx and their constitutent minerals systematically display preferential enrichments in highly incompatible and fluid mobile elements [*Khedr et al.*, 2013; *Khedr et al.*, 2014; *Prigent et al.*, 2018a]. The sole is composed of slivers of metamorphosed mafic crust with subordinate metasediments and serpentinites stripped from/by the understhrusted lithosphere. It is characterized by an inverted metamorphic gradient, from low temperature (LT) greenschist facies at the base up to high temperature (HT) amphibolite/granulite facies at the upper contact with the ophiolite mantle [*Ghent and Stout*, 1981; *Searle and Cox*, 1999; *Soret et al.*, 2017]. Geochronology indicates that peak HT metamorphism is only 1-2 My younger than the ophiolite crustal sequence (96.16-94.82Ma [*Rioux et al.*, 2016; *Warren et al.*, 2005]) suggesting that the overlying mantle lithosphere was young and hot when the metamorphic sole formed.

Listvenites outcrop irregularly along the basal thrust of the the Semail Ophiolite, often as 2-50 m bodies within the highly altered ophiolitic and sedimentary mélange in contact with its metamorphic sole (Fig 1a; [*Glennie et al.*, 1974; *Nasir et al.*, 2007; *Stanger*, 1985; *Wilde et al.*, 2002]). One of the largest listvenite bodies outcrops over ~1 x 2 $km^2$ in the Wadi Mansah area (South of Muscat). It comprises large lenses of serpentinites and marks the transition from mantle peridotites to greenschist facies meta-basalts and silicic sediments [*Falk and Kelemen*, 2015; *Villey et al.*, 1986]. This site was chosen to drill OmanDP Hole BT1B with the objective to sample the transition from the ophiolite mantle section to its metamorphic sole.

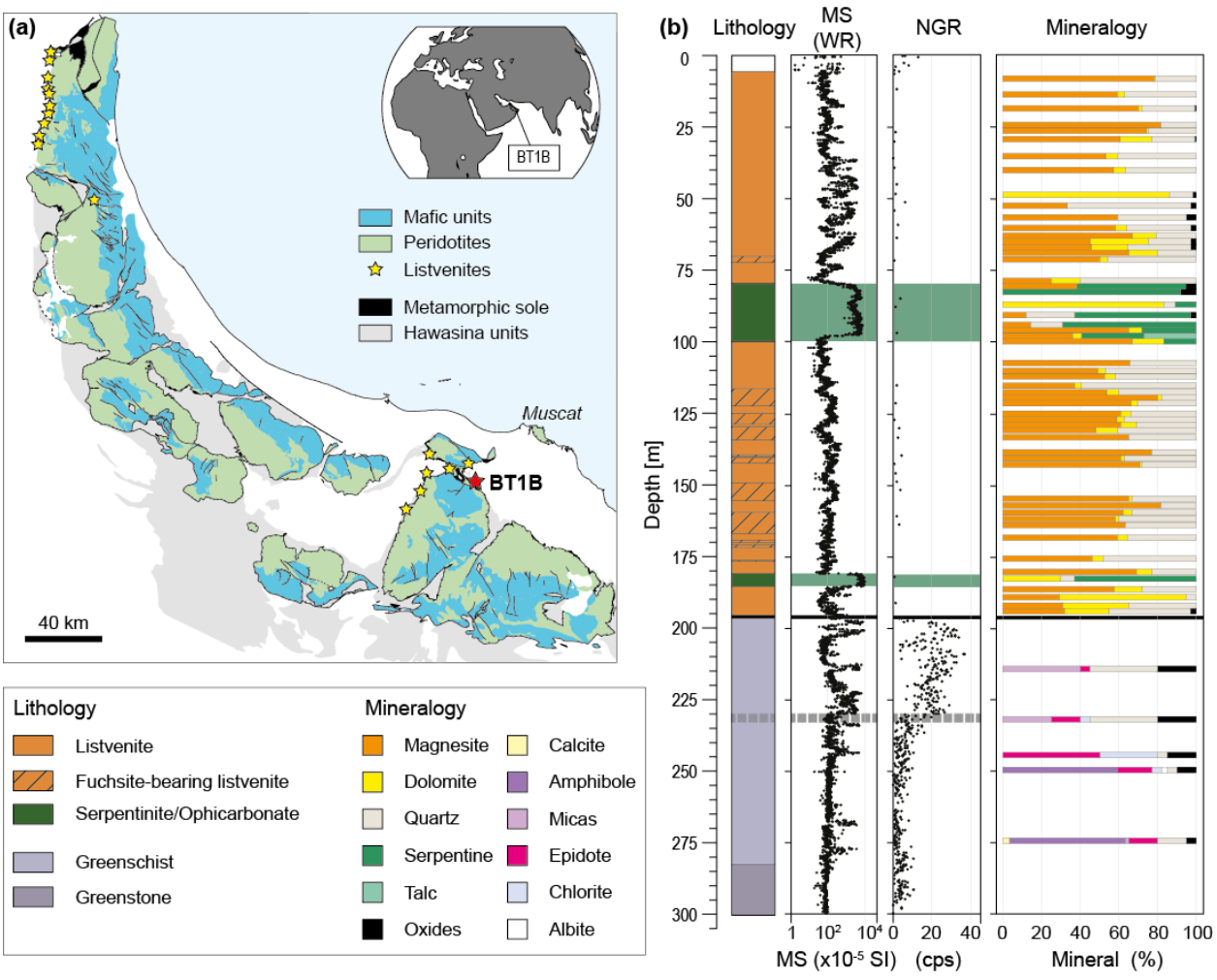


**Figure 1**. Location and downhole plots of lithological and physical properties of OmanDP Hole BT1B. (a) Simplified geological map of the Samail ophiolite in the Sultanate of Oman. Location of OmanDP Hole BT1B and regional occurrences of listvenites (after Boudier and Nicolas [2018]) represented by red and yellow stars respectively. (b) Downhole plots of drilled lithologies, magnetic susceptibility (MS), natural gamma rays (NGR), and mineral proportions (data from Kelemen et al [2020b]). Plotted mineral proportions correspond to XRD analysis wherever it is available and otherwise, thin section observations.

## 2.2 OmanDP Hole BT1B and sampling

Drilling at OmanDP Hole BT1B (23°3607 N, 58°.1887 E) recovered 300.05 meters of continuous cores. The mineralogy, alteration and structure of the cores and their main physical and chemical properties were measured on-board D/V Chikyu on whole cores, core sections (Visual Core Description — VCD) and thin sections [*Kelemen et al.*, 2020b]. The main characteristics of the cores are summarized here.

Below a few meters of alluvial material, Hole BT1B drilled through first a series of listvenites interlayered with serpentinites (hereafter grouped as the *listvenite series*), then through the basal thrust at ~197 meters below ground (mbg) and, finally, into the metamorphic sole (Fig. 1b).

Listvenites comprise dominantly magnesite ± dolomite and quartz, and are characterized by their pale yellow to dark reddish brown color in hand specimen. They contain relicts of chromian spinel and magnetite alignments indicating that their protolith was a serpentinized peridotite [*Beinlich et al.*, 2020; *Kelemen et al.*, 2020b]. Between ~ 110 and 182 mbg, fuchsite, a chromian mica, is commonly observed; it occurs as light green quartz-fuchsite intergrowths forming mm- to cm-size green spots easily recognizable on hand samples. Listvenites are highly brecciated down to ~80 mbg and the presence of highly weathered fragmented veins and breccia, associated with occurrences of hematite and goethite, results in variable and sometimes high magnetic susceptibility (Fig. 1b).

Serpentinites have dark- to olive-green colors and high magnetic susceptibility values (Fig. 1b). They were recovered at 80.28-100.23 mbg and 181.26-185.47 mbg. Serpentinites are foliated to massive, they have mesh textures outlined by magnetite, and bastite is commonly observed. They are crosscut by abundant light-green to white veins of dolomite (± magnesite) and serpentine with, locally, carbonates replacing the serpentine matrix. Variously carbonated serpentinites are distinguished from listvenites by the absence of quartz, but minor talc is found locally at ~98–100 mbg, close to the contact with listvenites.

The metamorphic sole is composed of greenish, microcrystalline and finely laminated schists (197.6-282.88 mbg) and greenstone (below 282.88 mbg) interpreted during shipboard logging as metasediments and metabasalts respectively. It comprises epidote, chlorite, albite, quartz, titanite, with carbonate and/or muscovite in schists and blue-green amphibole and minor pumpellyite in greenstones. The contact with the upper listvenite series occurs at 196.56-197.6 mbg. This tectonic contact consists of a ~0.6 m thick layer of fault gouge mixed with clasts of highly fragmented, fine-grained, chlorite- and epidote-bearing rocks. The thrust is characterized by a strong and sharp increase in the Natural Gamma Radiation values (NGR), jumping from on average <1 cps (counts/s) in the upper parts of Hole BT1B to >30 cps at the thrust, then gradually decreasing downhole over ~30-40 m to relatively homogeneous and low values (<5 cps) (Fig. 1b).

84 samples were collected from Hole BT1B for bulk rock geochemical measurements. Due to the high petrographic variability of the core, the VCD rock-names were used to designate geochemistry samples. 51 listvenites, 14 serpentinites, and 19 greenshists and greenstones were analyzed. 15 samples were collected on-site every 20m during the drilling operations. During the description of the cores on board D/V Chikyu, 59 samples were selected by the shipboard science party as representative of the different lithologies recovered from Hole BT1B. 10 additional listvenites and serpentinites were selected from Sections C5704B-73Z-1 to -75Z-2 (180.01-186.945mbg) for a coordinated on-shore study of the lower serpentinite intervals and neighboring listvenites (thereafter referred to as consortium samples).

## 3 Methods

The major element composition of BT1B samples was determined by X-ray fluorescence (XRF) on-board D/V Chikyu for the drillsite and shipboard samples and at GeoLabs (Ontario, Canada) for consortium samples. Total $H_2O$ and $CO_2$ concentrations and abundances in inorganic carbon of the drillsite and shipboard samples were determined by combustion CHNS elemental analysis (EA) and coulometry, respectively, on-board D/V Chikyu. The FeO concentrations of a subset of samples (8 serpentinites and 21 Listvenites) was quantified at the University of Lausanne (ISTE) following the Fe-titration protocol of Wilson [1960]. The trace element

composition (Li, Sc, Ti, V, Mn, Co, Ni, Cu, Ga, As, Sn, Sb, Rb, Sr, Y, Zr, Nb, Cs, Ba, Rare Earth Elements (REE), Hf, Ta, Pb, Th, U, W) of the drillsite, shipboard and consortium samples was analyzed by Inductively-Coupled-Plasma-Mass Spectrometry (ICP-MS) at Géosciences Montpellier (AETE-ISO Facility, University of Montpellier, France) using the protocol described in Godard et al. [2000]. The preparation of the samples and the analytical procedures are detailed in Supporting Information S1. The main lithological characteristics of the studied samples and their major, trace and volatile element concentrations are reported in Supplementary Dataset S1.

## 4 Results

The listvenite series and the underlying metamorphic sole are distinguished by significant downhole differences in the values of several geochemical indicators, such as loss on ignition (LOI), Mg# (100 x cationic (Mg/(Mg+Fe), with all Fe as $Fe^{2+}$), $Al_2O_3$ and trace element contents as illustrated on Figs. 2 and 3. These variations allow to discriminate several lithological and geochemical domains along Hole BT1B.

### 4.1 Geochemistry of the listvenite series (depth: 6.02-196.56 mbg)

The listvenite series are characterized by high LOI (13.1-46.8 wt.%), high Mg# (~90), high concentrations in transition metals such as Ni (up to 3110 ppm), Co (up to 128 ppm) and Cr (up to 4050 ppm), low concentrations in $Al_2O_3$ (<2 wt.%), $Na_2O$ (~0.1 wt.%) and $TiO_2$ (<0.1 wt.%) and in incompatible lithophile trace elements, such as Th (<<0.005 ppm), REE (ΣREE <1 ppm) and high field strength elements (HFSE, e.g., Zr~0.1 ppm). These compositions are highly variable downhole at the sample- to the meter scale yet they overlap, on average, that of the Semail ophiolite mantle (Figs. 2-5).

Volatile elements dominate the composition of the listvenite series (LOI = 13.1-46.8 wt.%). Listvenites have high $CO_2$ indicative of the predominance of carbonates (LOI>21.2 wt.%; $CO_2$=21.3-43.2 wt.%) but no $H_2O$ (~0 wt.%). Serpentinites display the highest $H_2O$ contents (up to 12.1 wt.%), primarily hosted by serpentines that structurally comprise ~13 wt.% $H_2O$ [*Deer et al.*, 1996], and they have the lowest LOI (down to 13.1 wt.%) and $CO_2$ (down to 5.6 wt.%). Carbonate-rich serpentinites have intermediate compositions with LOI up to 36.1 wt.%, $CO_2$ up to 33.1 wt.% and $H_2O$ as low as 0.3 wt.%. Correlated TIC and total carbon values allow to distinguish samples in which dolomite represent the dominant carbonate species as the shipboard coulometry protocol did not allow the complete dissolution of magnesite (see Supporting Information S1). Most of these samples are serpentinites ($CO_{2(TIC)}$ up to 33.3 wt.%; $CO_{2(TIC)}$: TIC recalculated as $CO_2$).

**Figure 2**. (next page) Concentrations of selected geochemical species plotted by depth downhole for all samples from Hole BT1B. Dashed line indicates the median concentration from literature data for peridotites from the main mantle section (MMS) of the Semail Ophiolite (n=92; [*Gerbert-Gaillard*, 2002; *Godard et al.*, 2000; *Hanghoj et al.*, 2010]), and the grey field indicates ± 1 standard deviation (calculated as the 16th and 84th percentile) about the median (Supplementary Table S2). Major oxides are plotted on a volatile free basis. Symbols are in inset. Listvenites, fuchsite-bearing listvenites (Fu-listvenites), serpentinites and ophicarbonates (grouped as Serpentinites) from Listvenite domains I, II and III (see text) are noted I, II and III respectively. Samples from the metamorphic sole (noted sole) are grouped, from top to bottom, as M1, M2 and M3 (see text)

275

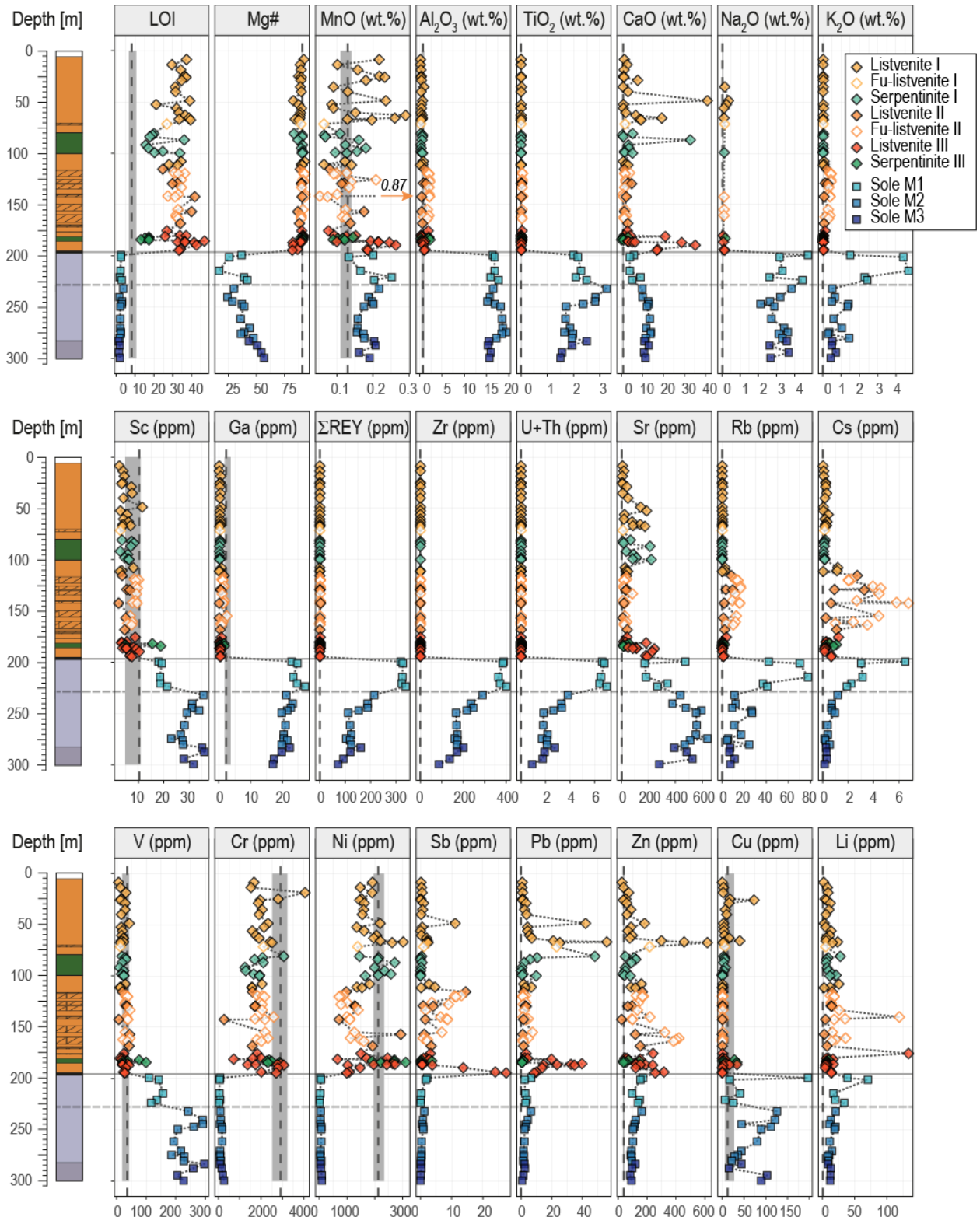
Depth [m]
LOI
Mg#
MnO (wt.%)
Al2O3 (wt.%)
TiO2 (wt.%)
CaO (wt.%)
Na2O (wt.%)
K2O (wt.%)
0.87
Listvenite I
Fu-listvenite I
Serpentinite I
Listvenite II
Fu-listvenite II
Listvenite III
Serpentinite III
Sole M1
Sole M2
Sole M3
Sc (ppm)
Ga (ppm)
ΣREY (ppm)
Zr (ppm)
U+Th (ppm)
Sr (ppm)
Rb (ppm)
Cs (ppm)
V (ppm)
Cr (ppm)
Ni (ppm)
Sb (ppm)
Pb (ppm)
Zn (ppm)
Cu (ppm)
Li (ppm)

276
277

In addition to volatile elements, listvenite series are composed mainly of Si, Mg, Fe and Ca: these elements calculated as oxides represent ~99 % of the volatile-free mass of samples. Their distribution relate primarily to the mineralogy of the core (Fig. 4a): variations in $SiO_2$ (4.4–70 wt.%) reflect changes in carbonate-quartz ratio in listvenites, and in carbonate-serpentine ratio in serpentinites while downhole spikes in CaO (up to 32.8 wt.% in the serpentinites and up to 40.9 wt.% in listvenites) correspond to increasing TIC values ($CO_{2(TIC)}$ up to 40.1 wt.% in listvenites), indicative of the presence of dolomite (Fig. 1; [*Kelemen et al.*, 2020a]). Relationships to mineralogy are more difficult to identify for Mg, Fe and Mg#, except for local decreases in MgO and Mg# associated to high CaO and TIC contents indicative of the presence of dolomite (e.g. listvenite C5704B-23Z-1-1,37.0--42.0cm at 48.72 mbg; Figs. 2-3). In contrast, $Al_2O_3$, transition metals (e.g., Ti, Ni and Co) and lithophile trace elements (e.g., REE, Y) do not correlate with changes in mineralogy and volatile chemistry: in particular, we do not observe major changes in their distribution between listvenites and serpentinites. These elements, generally considered as fluid-immobile, display coherent tens of meter scale downhole trends that allow to define three geochemical domains (Figs. 3-5), thereafter described as, from top to bottom, listvenite domains I, II and III.

*Listvenite domain I* (top to~112 mbg) comprises listvenites (*listvenites I*), including one fuchsite-bearing listvenite, and serpentinites (*serpentinites I*). It is characterized by low concentrations of $Al_2O_3$ (0.14-0.92 wt.%) and $TiO_2$ (<0.01 wt.%) and of trace elements (e.g. $Yb_N$=0.03-0.22; N=normalized to CI-Chondrite [*McDonough and Sun*, 1995]) that overlaps that of the harzburgites and dunites from the main mantle section (MMS) of the Semail ophiolite [*Godard et al.*, 2000; *Hanghoj et al.*, 2010; *Lippard et al.*, 1986]. It displays relatively linear REE patterns similar to that of the MMS, with normalized REE abundances decreasing from heavy (HREE) to light REE (LREE) ($[Ce/Yb]_N$=0.08 – 0.54). Several samples, in particular the serpentinites and ophicarbonates, present minor LREE enrichments relative to middle REE (MREE) (e.g., carbonate rich serpentinite C5704B-44Z-4, 50.0-55.0 cm with $(La/Sm)_N$=3.7), similar to what observed in some Ca-bearing carbonates from oceanic and ophiolitic low temperature peridotite hosted hydrothermal systems [*Noel et al.*, 2018; *Schroeder et al.*, 2015].

*Listvenite domain II* (~112 mbg to ~170 mbg) is composed of listvenites alternating with fuchsite-bearing listvenites (all grouped as *listvenites II*). It is characterized by an elevated concentrations of $Al_2O_3$ (0.4-2.23 wt.%) and $TiO_2$ (0.02-0.06 wt.%) compared to Listvenite domain I. This domain has higher lithophile trace element contents (e.g. $Yb_N$=0.18-1.03) and highly fractionated "spoon-shaped" REE patterns ($(Ce/Yb)_N$=0.007-0.061) with relatively flat convex-upward MREE-HREE segments ($(Dy/Yb)_N$=0.49-0.96) and slight but systematic enrichments of La relative to Ce ($(La/Ce)_N$=1.03-4.9), comparable to that of the basal lherzolites and amphibole-bearing basal lherzolites from the northern Semail ophiolite (Figs. 4-5; [*Khedr et al.*, 2014; *Takazawa et al.*, 2003]). These REE patterns are very similar in shape to those obtained by Prigent et al [2018a] on clinopyroxene and amphibole from the banded lherzolite units close to the metamorphic sole. Listvenite domain II is also distinguished by, on average, low Ni (~1200 ppm) and Co (~68 ppm) concentrations and low $Fe^{3+}/Fe_{TOT}$ (0.1-0.6) compared to Lisvenite domain I (Ni~1900 ppm; Co~90 ppm; $Fe^{3+}/Fe_{TOT}$~0.7).


**Figure 3**. Concentrations of selected geochemical species plotted by depth downhole for samples from the Hole BT1B listvenite series only. Dashed grey and green lines indicates the median concentration from literature data for peridotites from the main mantle section (MMS, n=92) and basal lherzolites ([*Lippard et al.*, 1986; *Takazawa et al.*, 2003]; n=13) of the Semail ophiolite, respectively. Fields of the corresponding color indicate ± 1 standard deviation (calculated as the 16th and 84th percentile) about the median (Supplementary Table S2). Symbols for Hole BT1B samples and literature data are in inset, abbreviations are as in Figure 2.

*Listvenite domain III* (~170 mbg to the basal thrust) is the closest to the metamorphic sole. It comprises listvenites (*listvenites III*) and serpentinites (*serpentinites III*). It has concentrations in $Al_2O_3$ (0.24-2.30 wt.%), $TiO_2$ (<0.02 wt.%) and of trace elements (e.g. $Yb_N$=0.05-0.77) intermediate between that of the Lisvenite domains I and II, the most enriched samples being serpentinites and listvenites close to Listvenite domain II. It displays linear REE patterns mostly similar to that of Lisvenite domain I ($(Ce/Yb)_N$=0.08-0.67) with the exception of some samples close to Listvenite domain II that have similarly fractionated REE patterns ($(Ce/Yb)_N$=0.011-0.163). Listvenite domain III is characterized by systematic enrichments in LREE relative to MREE ($(La/Sm)_N$=0.34-3.29), this trend overall increasing towards the basal thrust. This downhole trend goes with a decrease in Mg# (down to 82), an increase in $Fe^{3+}/Fe_{TOT}$ up to Listvenite domain I values (0.38-0.83) and an increasingly scattered distribution for several elements such as Ni (650-3100 ppm) and Co (35-128 ppm), or Cu (0.2-34 ppm) and Pb (0.5-39.7 ppm) as well as a progressive increase in the concentrations of CaO (up to 35.1 wt.%), Sr (up to 244.3 ppm) and Sb (up to 27.4 ppm). These variations are associated to an increase in the dolomite fraction towards the basal thrust (Fig. 1b).

The listvenite series display spiked U-shaped trace element patterns that reflect the relative depletion of Zr-Hf relative to neighboring elements and significant enrichments in incompatible fluid mobile elements (FME), such as alkali elements (Cs, Rb, Ba), Li, Sb, U, Pb and Sr relative to Th, Nb, Ta and LREE (Fig. 5). These strong FME enrichments distinguish the listvenite series from refractory peridotites from the main mantle section (Figs. 2, 3 and 5). High FME concentrations appear as spikes on downhole plots (Fig. 3). These spikes are however located preferentially in well-defined listvenite domains for most elements with a decoupling in the downhole distribution of alkali elements and other FME such as Sb, Pb, Sr and U. High concentrations of alkali elements including $K_2O$ (0.07-0.45 wt.%), Ba (up to 420 ppm), Rb (1.1-17 ppm) and Cs (0.24-6.8 ppm) distinguish Listvenite domain II from Listvenite domains I and III ($K_2O$=0.02-0.08 wt.%; Rb=0.006-2.6 ppm; Cs=0.02-1.19 ppm), with the highest concentrations in fuchsite-bearing listvenites. In contrast, downhole spikes in concentrations for Pb, Sr and U are mainly in Listvenite domains I and III (Pb up to 56 ppm, Sr up to 244 ppm, U up to 0.04 ppm). Cu (up to 73 ppm) and to a lesser extent, Sb (up to 27.4 ppm) and Zn (up to 610 ppm) display similar trends with peaks in concentrations mainly in Listvenite domains I and III.

For some elements, their concentrations and distribution are highly scattered and become virtually indistinguishable from the metamorphic sole, as for Li and MnO (e.g., Li=2.5-134 ppm in listvenite series and 8-70 ppm in metamorphic rocks; Fig. 2). Some of these extreme enrichments can be correlated on a case-by-case basis to lithological or structural features as for MnO-rich sample C5704B-60Z-4-1,24.0--29.0 cm(V) (MnO=0.87 wt.%) identified as a listvenite vein crosscutting a fuchsite-bearing listvenite (C5704B-60Z-4-1,24.0--29.0cm(H)). This sample is also the most enriched in REE and Y (e.g., Y=2.2 ppm) and the most depleted in Cr (271 ppm) indicating extensive elemental redistribution occurring at the sample scale.

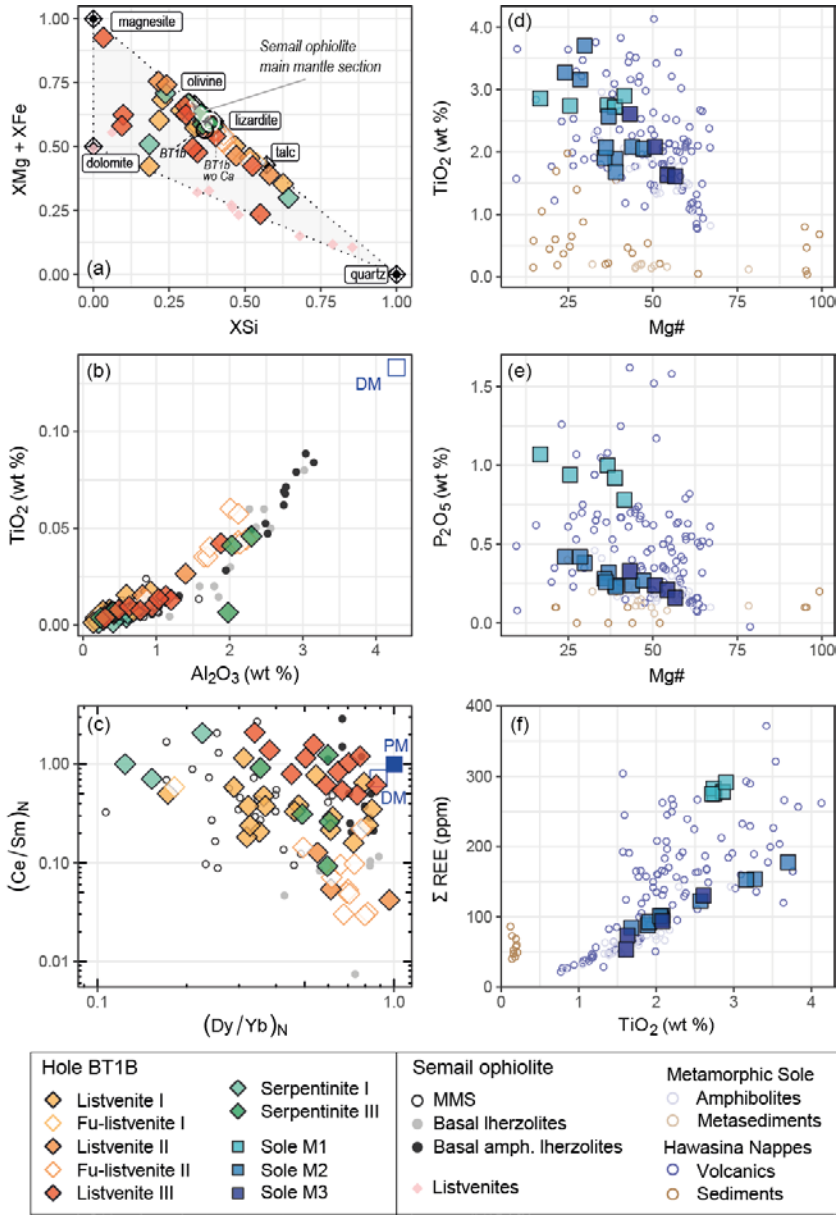


**Figure 4**. Scatterplots of the composition of samples recovered from Hole BT1B. The composition of the listvenite series is plotted as (a) (XMg + XFe) versus XSi (X = molar proportion), (b) $TiO_2$ (wt.%) versus $Al_2O_3$ (wt.%), (c) Chondrite normalized (La/Sm) versus (Dy/Yb) diagrams. The composition of the metamorphic sole is plotted as (d) $TiO_2$ (wt.%) and (e) $P_2O_5$ (wt.%) versus Mg# and on (f) Total REE (ppm) versus $TiO_2$ (wt.%) diagrams. (a) The composition of the listvenite series is compared to the range of compositions of refractory peridotites from the Semail Ophiolite (white field) and to the composition of magnesite, dolomite, quartz, talc, lizardite and olivine [*Deer et al.*, 1996], the mean composition of listvenite series (black circle) also, recalculated as Ca free (white circle). (b)$TiO_2$ and $Al_2O_3$ compositions are plotted on a volatile-free basis and, when available, recalculated ICPMS data was used for plotting $TiO_2$. The composition of depleted mantle (DM [*Salters and Stracke*, 2004]) and primitive mantle (PM [*McDonough and Sun*, 1995]) and/or literature data from the Semail mantle (MMS [*Gerbert-Gaillard*, 2002; *Godard et al.*, 2000; *Hanghoj et al.*, 2010], basal

lherzolites [*Lippard et al.*, 1986; *Takazawa et al.*, 2003] and amphibole bearing basal lherzolites – Basal amph. lherzolites [*Khedr et al.*, 2014]) and listvenites [*Falk and Kelemen*, 2015] are shown for comparison on (a), (b) and (c). The composition of Permian and Triassic volcanics (including Haybi) ([*Chauvet et al.*, 2011; *Lapierre et al.*, 2004; *Lippard et al.*, 1986; *Maury et al.*, 2003]) and sediments [*Oberhänsli et al.*, 1999] from the underthrusted Hawasina nappes, and of amphibolites and metasediments from the metamorphic sole [*Ishikawa et al.*, 2005] are shown for comparison on (d) , (e) and (f). Symbols are in inset and abbreviations are as in Figure 2.

### 4.2 Geochemistry of the metamorphic sole (depth: 196.56- 300.13 mbg)

BT1B metamorphic rocks have LOI of 1.3-3.8 wt.% related to the presence of $H_2O$ (>2 wt.%) in hydrous minerals (chlorite, amphibole …) and minor $CO_2$ (0.04-0.97 wt.%) in carbonates, mainly calcite ($CO_{2(TIC)}$ 0.01-0.95 wt.%). Compared to listvenite series, they have low Mg# (16.7-56.6), low concentrations of Cr (42-265 ppm) and Ni (15-86 ppm) and high concentrations of $Al_2O_3$ (15.2-19.4 wt.%), $Na_2O$ (2.1-4.7 wt.%), $P_2O_5$ (0.16-1.07 wt.%) and $TiO_2$ (1.6-3.7 wt.%) and they display a relatively narrow range of $SiO_2$ concentrations (44.5-52.6 wt.%). They are characterized by high concentrations of V (110-297 ppm) and of incompatible trace elements, such as Th (0.75-5.9 ppm), REE (ΣREE=54-291 ppm) and HFSE (e.g., Nb=9.5-63 ppm), and by LREE-enriched chondrite–normalized REE patterns $(Ce/Yb)_N$=3.4-8.2). They overlap in composition with the amphibolites from the Semail ophiolite metamorphic sole [*Ishikawa et al.*, 2005; *Lippard et al.*, 1986] and the volcanic rocks from the underthrusted Hawasina assemblages [*Chauvet et al.*, 2011; *Lapierre et al.*, 2004; *Maury et al.*, 2003] (Figures 4-5). More particularly, they display trace element compositions similar to the transitional to alkali basalt series forming the Hawasina-Haybi complex, suggesting that the metamorphic rocks recovered at Hole BT1B comprise only metabasalts. We have subdivided the Hole BT1B metamorphic rocks into three groups based on their lithology, physical properties, geochemistry and depth (Fig. 3).

The first group (*M1*) corresponds to the high NGR cores (197.6-~230 mbg; Fig. 1b). It represents the most enriched endmember of BT1B metabasalts for $P_2O_5$ (0.78-1.07wt.%), for alkali elements ($K_2O$=1.5-4.7wt.%; Ba=192-598ppm; Rb=37-78ppm; Cs=1.9-6.5ppm) and for moderately to highly incompatible lithophile elements, such as REE ($Yb_N$~23), Th (5.1-5.9ppm) and U (1.0-1.3ppm). They have however middle range values for transition elements $TiO_2$ (1.9-2.4wt.%), V (110-157ppm) and Sc (17.9-21.3ppm). They are overall depleted in CaO (3.95-9.1wt.%) and in Sr (173-342ppm) although these elements increase with depth. *M1* metabasalts display the most fractionated REE patterns ($(Ce/Yb)_N$=7.7-8.2) as well as slight enrichments in Nb-Ta (e.g. Nb/Th~1.27xPM), and negative anomalies in Pb and Sr relative to neighboring elements (Pb/Ce~0.25xPM; Sr/Ce 0.2xPM) on extended trace element diagrams (Fig. 5). Their high concentrations in K, Th and U likely explain their high NGR values (Fig.1).

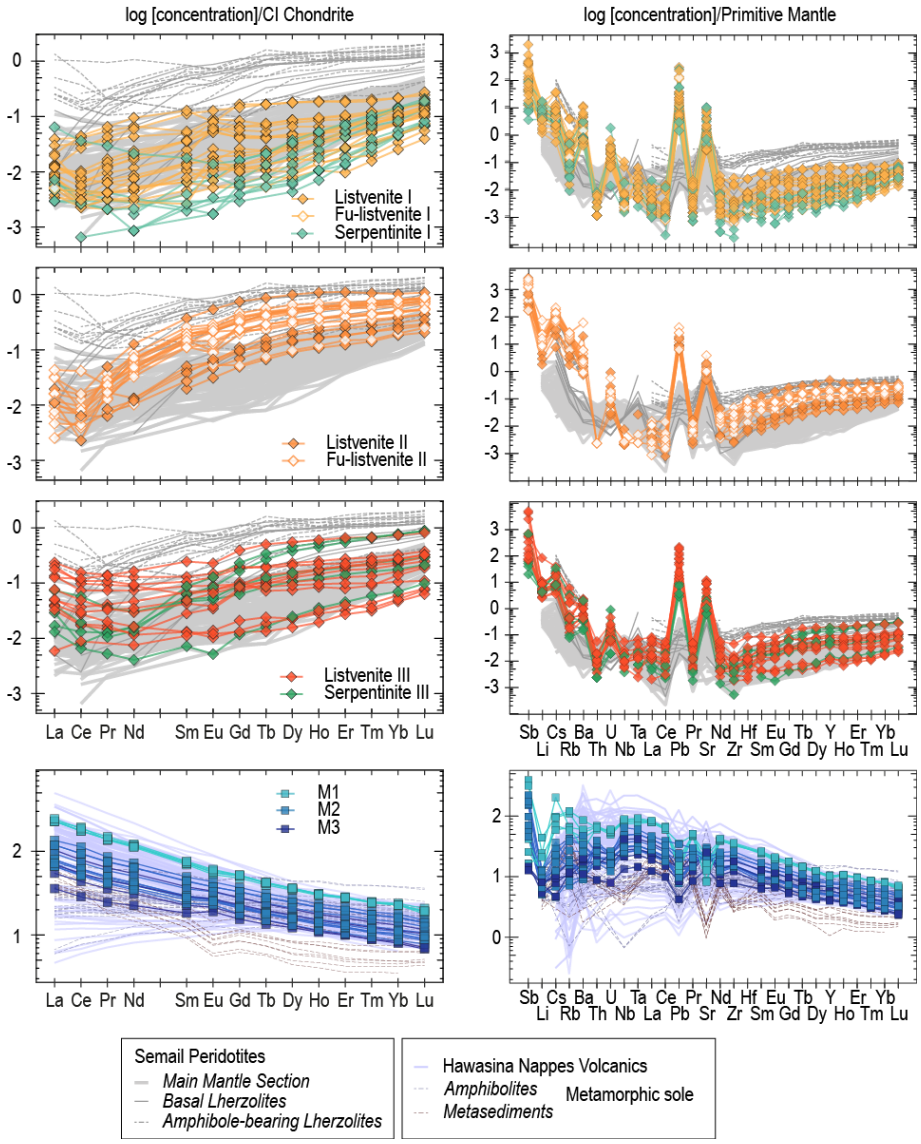


**Figure 5**. Rare-earth element (REE) and trace element spider diagrams for samples from Hole BT1B. Separate panels are plotted for Listvenite domains I, II and III (see text), and for the metamorphic sole. Left: CI chondrite-normalised REE patterns. Right: Primitive mantle-normalized trace element plots; normalizing values from McDonough and Sun [1995] . Literature data from Semail Ophiolite peridotites are plotted for reference in the upper three panels, and from metamorphic sole and Hawasina nappes in the lowermost panel. Symbols are in inset. Abbreviations are in Figure 4.

The second and third groups, *M2* (~230–282.88 mbg) and *M3* (below 282.88 mbg) are composed of schists and greenstones respectively. The downhole transition from *M1* to *M2-M3* metabasalts is characterized by a sharp decrease in $K_2O$, and Rb, REE, HFSE, Th and U and a sharp increase in $TiO_2$ (up to 3.7 wt.%; Fig.2). *M2-M3* metabasalts record a continuous downhole increase in Mg# (up to 56.6), Sc (up to 36 ppm), V (up to 297 ppm), Co (up to 45 ppm) and Ni (up to 87 ppm) and a decrease in alkali elements (e.g., $K_2O$ down to 0.3 wt.%) and

in moderately to highly incompatible lithophile elements (e.g., $TiO_2$ down to 1.6 wt.%; Th down to 0.7 ppm). They also show a continuous decrease in trace element concentrations and in LREE/HREE ratios with depth (*M2:* $Yb_N$ = 17.7-8.5, $(Ce/Yb)_N$=6.4-4.5; *M3:* $Yb_N$ = 13.1-8.3, $(Ce/Yb)_N$=6.0-3.4; Figs. 2, 4). Negative correlations between $TiO_2$, REE and HFSE and Co, Ni and Mg# such as those observed downhole are typical of basaltic fractional crystallization trends with the lowermost *M3* metabasalts having the least evolved compositions. Finally *M2-M3* metabasalts display positive anomalies in Nb-Ta (e.g. Nb/Th~1.5xPM), minor negative anomalies in Pb (Pb/Ce=0.43-0.88xPM) and variable Sr anomalies (Sr/Ce=0.5-1.7xPM) relative to neighboring elements on extended trace element diagrams (Fig. 5). It should be noted also that CaO and Sr downhole trends appear decoupled from other elements: they increase then stabilize with depth in *M2* (CaO up to 14.0 wt.%; Sr up to 638 ppm) and decrease towards the bottom of the borehole (CaO down to 10.75 wt.%; Sr down to 281 ppm).

## 5 Discussion

Drilling at Hole BT1B provides the first high resolution sampling of the transition from the base of the Semail ophiolite to its metamorphic sole, thus allowing a detailed study of the mineralogical and geochemical processes occurring across this major tectonic structure. The basal thrust constitutes the ophiolite sole in this area and separates highly metasomatized, deformed and fractured rocks of the mantle-derived listvenite series from the underlying greenschist lithologies. The listvenite series recovered from the upper ~200 m of Hole BT1B comprise highly fractured and veined listvenites and fuchsite-bearing listvenites and two minor intervals of variously carbonated serpentinites (Fig. 1). Their main petrophysical and geochemical characteristics reflect the dominant mineralogy of the cores: quartz + magnesite ± dolomite ± fuchsite for listvenites; and serpentine ± dolomite ± magnesite for carbonated serpentinites (Figs. 1-4). Specifically, they have high $CO_2$ contents (up to ~43 wt.%, Fig. 3) showing the ubiquity of fluid-rock interactions with $CO_2$-bearing fluids (Kelemen et al [2021] and references therein). In spite of the complete transformation of their mineralogy due to $CO_2$-metasomatism, the listvenite series have average compositions comparable to that of the highly serpentinized, often amphibole bearing, banded lherzolites forming a narrow zone at the basal transition from the Semail mantle section to its metamorphic sole (Fig. 2-5, [*Khedr et al.*, 2013; *Khedr et al.*, 2014; *Prigent et al.*, 2018a; *Yoshikawa et al.*, 2015]). The BT1B metamorphic rocks recovered in the lower ~100m of the borehole comprise finely laminated, fine grained greenish mineral assemblages. They have basaltic compositions similar to that of the alkali basalts from the underthrusted Hawasina assemblages (Figures 4-5) from which they likely derive (e.g., [*M P Searle and Malpas*, 1980]). There is no compositional evidence for the presence of interlayered meta-sediments, which are often observed associated with the mafic amphibolites composing the metamorphic sole elsewhere in Oman (e.g., [*Agard et al.*, 2016; *Cowan et al.*, 2014; *Lippard et al.*, 1986; *Soret et al.*, 2017]) including in Wadi Mansah [*Falk and Kelemen*, 2015], and as previously hypothesized for BT1B cores [*P.B. Kelemen et al.*, 2020a]. They display decreasing concentrations in alkali elements from *M1* to *M2-M3* metabasalts, similar to others have been observed in the metamorphic sole, associated with the transition from HT to LT away from the ophiolite contact ([*Ishikawa et al.*, 2005]; Fig. 2), although the mineralogy of those lithologies indicate equilibration mainly under greenshist facies, indicative of retrograde metamorphism (e.g., [*Ambrose et al.*, 2021; *Ghent and Stout*, 1981]).

We will use the high resolution geochemical database to evaluate the mass and volume changes associated to the formation of the listvenite series during $CO_2$ metasomatism and discuss

elemental mobility during these processes. We will focus in particular on the role of the composition of the (metasomatized) protolith(s), the main fluid pathways as recorded across the basal thrust and possible changes in fluid source(s) and interactions with adjacent lithologies.

### 5.1 Mass changes and elemental mobility during listvenization

To evaluate the respective contribution of the host rock and incoming metasomatic fluids(s) to the composition of the listvenite series and to constrain elemental mobility at the scale of the borehole, we used the mass balance model of Baumgartner and Olsen [1995]. This approach allows to evaluate the addition and removal of a broad range of chemical elements during the alteration of a protolith of known composition and the resulting mass changes, without a priori assumptions on elemental mobility. The main challenge for these calculations was determining consistent and representative trace element compositions for the listvenite series and for the model protoliths.

The listvenite series are characterized by strong downhole variations in mineralogy and geochemistry from the sample to the meter scale. For simplicity, mass balance calculations (detailed in Supplementary Information Text S2) were carried out for the two main rock types, (listvenites including fuchsite-bearing listvenites, and the variously carbonated serpentinites), for each of the downhole geochemical listvenite domains I, II and III. The results are illustrated as isocon diagrams (Fig. 6) where average elemental concentrations of the altered rock are plotted against those of the model protolith. Immobile elements were identified on the basis of the largest number of elements which are consistent with a single isocon (line of immobility) to within their uncertainty in the protolith and altered rock (i.e. collinear on the plot). The 1:1 reference line on isocon diagrams corresponds to zero mass change during alteration. Isocons which lie above or below the 1:1 line indicate, respectively, overall mass loss or mass gain during alteratio (reflecting overall concentration or dilution of immobile elements during each of these scenarios). Elements plotting above and below the isocon are enriched and depleted, respectively, in the altered rocks compared to the model protolith.

The trace element compositions for the model protoliths were determined on the basis of the published geochemical studies of Semail peridotites for which structural (localization, distance to the Moho and/or to the sole) and petrological (lithology, mineralogy) information were available. We defined two endmember compositions (Table S3): (1) a refractory protolith composition; due to the scarcity of data on the composition of basal peridotites, we used the data obtained on harzburgites ± dunites dominant in the main mantle section of the Semail ophiolite [*Gerbert-Gaillard*, 2002; *Godard et al.*, 2000; *Hanghoj et al.*, 2010; *Lippard et al.*, 1986]; (2) a fertile protolith, representative of the composition of basal lherzolites, including amphibole-bearing samples [*Khedr et al.*, 2014; *Lippard et al.*, 1986; *Takazawa et al.*, 2003]. The model refractory and fertile protoliths are noted MMS and basal lherzolite respectively in Fig. 6 and Table 1. It should be noted that, for some trace elements, the published chemical database is limited (e.g., Ga) and/or highly variable (e.g., LREE, Cs), in particular for basal lherzolites, resulting in a large uncertainty in their distribution in the model protolith(s); however, these elements represent a minor subset of the chemical database and therefore had little impact on the evaluation of the overall mass changes resulting from $CO_2$ metasomatism.

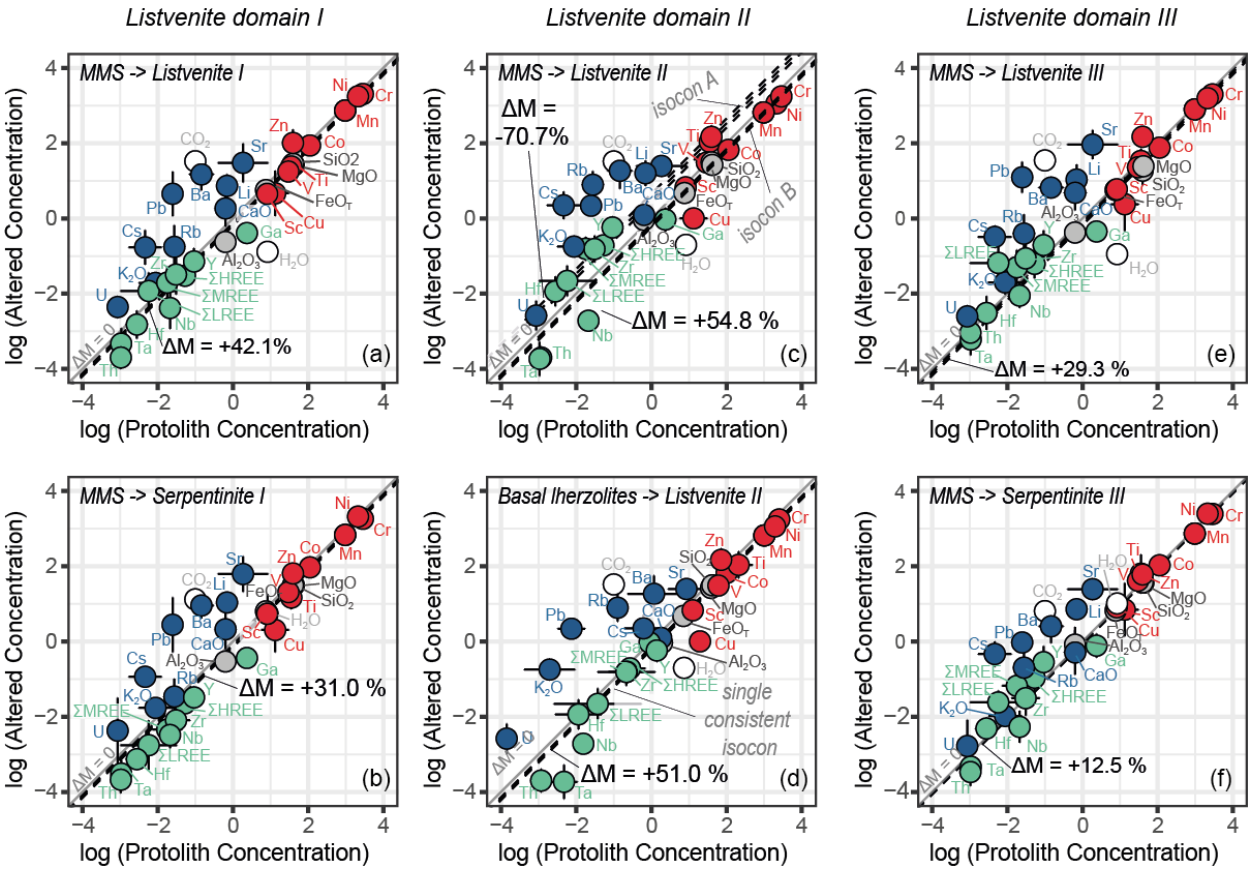


**Figure 6**. Mass balance diagrams for listvenite series from Hole BT1B. Isocon plots comparing the average composition of listvenites and serpentinites – calculated as the log normal mean – from each listvenite domains with potential protolith compositions on log-log scales. Plotted on each panel, each corresponding to a protolith–altered rock pair, is an isocon (line of immobility). Isocons were calculated using the approach of Baumgartner and Olsen [1995]. The 1:1 reference line in grey on each panel corresponds to zero mass change during alteration. Isocons above and below this indicate mass loss and gain, respectively. Using the average composition of the MMS refractory peridotites (calculated as the log normal mean) as the protolith composition for each domain, this approach gives consistent patterns of mobile and immobile elements, with the exception of Listvenites II (panel c) where two potential isocons are apparent in the data (labeled A and B). Mass balance was repeated for Listvenite II with the average composition of basal lherzolites (including amphibole bearing lherzolites) which gives a single consistent isocon and similar patterns of mobility/immobility to the other panels. Modeled protolith compositions and calculated statistics are in Supplementary Table S3.

The mass balance calculations comparing the composition of listvenites and serpentinites to the refractory protolith showed co-linearity (within uncertainty) for most major and trace elements on isocon diagrams (Fig. 6, Supplementary Information Text S2). Only listvenites II displayed inconsistent results with two parallel 1:1 slopes (Fig. 6c). The same calculations using the fertile model protolith showed collinear trends and elemental variations similar to those obtained for the adjoining domains (Fig. 6d). This result supports the hypothesis that the

listvenite series were formed after a mantle section having a structure and composition analogous to basal banded lherzolites, with Listvenite domains I and III being formed after a refractory protolith end-member, and Listvenite domain II after a fertile protolith.

The listvenite series do not record major changes in $SiO_2$, MgO and $FeO_T$, the main constituents of their mantle protolith(s), as already pointed out by Falk and Kelemen [2015] for the Wadi Mansah listvenites. Our new data show that $Al_2O_3$ and $Na_2O$, and transition elements generally concentrated in mantle peridotites (V, Cr, Co, Ni, Mn Ti, and Sc) are also immobile at the scale of the borehole despite their meter-scale scattered downhole distribution (Fig. 2 and 3). Similarly, moderately incompatible lithophile trace element such as HREE, MREE, Y, Zr and Hf are aligned on the same 1:1 trend indicating that they were immobile at the scale of the borehole during listvenitization. However, the most incompatible elements, even those generally considered as fluid immobile, display minor differences from one rock type and domain to the other (e.g., depleted LREE in Serpentinite I). In particular, Nb, Ta and Th are systematically depleted relative to the model mantle protoliths. This could reveal trace element depleted protoliths compared to the models but, we posit that it most likely relates to the uncertainty due to the limited dataset on the composition of these elements in the Semail peridotites. The same consideration could explain the apparent systematic loss of Ga observed for all calculations.

| Listvenite Domain | Lithology | Protolith | Mass change | Volume change |
|---|---|---|---|---|
| I | Listvenite | MMS | **42.1 ± 12.5** | 41.3 ± 14.4 |
| | Serpentinite | MMS | **31.0 ± 10.9** | 34.6 ± 13.6 |
| II | Listvenite | Basal lherzolites | **51.0 ± 13.3** | 50.1 ± 15.9 |
| III | Listvenite | MMS | **29.3 ± 20.2** | 28.8 ± 20.5 |
| | Serpentinite | MMS | **12.5 ± 4.5** | 13.9 ± 5.6 |

**Table 1.** Summary of mass and volume changes associated with $CO_2$ metasomatism. Changes in mass were determined from a mass balance calculations using the approach of Baumgartner and Olsen [1995]. These were converted to volume changes using a density of 2.81 ± 0.50 g $cm^{-3}$ for serpentinised peridotite protoliths [*Dewandel*, 2002] and the mean density of listvenite and serpentinite measured in BT1B cores, 2.86 ± 0.07 g $cm^{-3}$ and 2.52 ± 0.05 g $cm^{-3}$, respectively [*Kelemen et al.*, 2020b] and propagating the associated uncertainties. For the listvenite or serpentinite of each domains, results are shown for the most appropriate protolith only (see Supporting Text S2 for details).

Only a limited number of elements show evidence for significant remobilization during $CO_2$-metasomatism, relative to the model mantle protoliths. Enrichments are seen in CaO (where dolomite is present), and most elements typically considered as fluid mobile: Li, K, Rb, Cs, Ba, Sr, Pb and U. These enrichments vary from one domain and rock type to the other thus suggesting downhole variability in fluid rock interactions (discussed in Section 5.2 below). The most noticeable enrichment is however that of $CO_2$. It is associated to the development of two reaction pathways for carbonation with, on one hand, the formation of variously carbonated serpentinites (Serpentinites I and III, Figs. 6b, f) and, on the other hand, that of listvenites (Listvenites I, II and III, Figs. 6a, d, e). Listvenites are distinguished from carbonated serpentinites by their depletion in $H_2O$, suggesting that $CO_2$ addition induced the release of $H_2O$.

This process has been documented in listvenites from different orogens (e.g., Atlin listvenites [*Hansen et al.*, 2005]): it could be a non-negligible dehydration mechanism for serpentinized peridotites.

Mass balance calculations indicate that $CO_2$ metasomatism resulted in an increase of the mass of the listvenite series compared to their refractory and/or fertile protoliths for serpentinites as well as for listvenites. The estimated mass increase was slightly less for carbonated serpentinites (12 to 31 %) than for listvenites (29.3 to 51.0 %). The density of carbonated serpentinites, listvenites and model protoliths being relatively close, these mass changes induced volume expansion of the same order of magnitude (Table 1). This massive increase in mass and volume was likely accommodated by the abundant veining characterizing the listvenite series; it suggests a strong coupling between carbonation reactions and fracturing during their formation. The high density veining network could be associated to (1) crystallization forces produced by the carbonation reactions (e.g., [*Jamtveit et al.*, 2008; *Lambart et al.*, 2018; *Ulven et al.*, 2014]) and/or (2) regional tectonics as, for instance, the development of local and transient extension areas during the earliest stages of convergence in forearc and/or protoarc environments (e.g. [*Reagan et al.*, 2017]), for which the Semail ophiolite could be an analogue (e.g., [*Belgrano et al.*, 2019; *Kelemen et al.*, 2021]).

### 5.2 The BT1B listvenite series: sampling the final stage of a protracted suite of fluid rock interactions

The BT1B listvenites series are characterized by strong mineralogical and compositional variations from the sample to the meter-scale (Figs 2-4; Supplementary Dataset S1). Significant variations in mass and volume are also observed at the tens of meter scale, from one Listvenite Domain to the other (Table 1). In the same way, the transition from listvenite series to the underlying metamorphic sole is sharp for structure, mineralogy and for geochemistry (with the exception of Ca and Sr). These jagged distributions indicate that elemental transport was limited, and fluid-rock interactions localized, along the section during $CO_2$ metasomatism and that $CO_2$-bearing fluid(s) did not originate directly from the underlying metamorphic sole. The main flow paths for $CO_2$ rich fluids were probably parallel to the basal thrust, in relation to the localization of brittle and/or cataclastic deformation (e.g., [*Menzel et al.*, 2020b]). They thus followed and, possibly reused, the same pathways as the fluids driving earlier metamorphic events affecting the basal ophiolitic mantle (e.g., [*Lippard et al.*, 1986; *Prigent et al.*, 2018b; *Yoshikawa et al.*, 2015]) and its metamorphic sole (e.g., [*Ambrose et al.*, 2021; *Ghent and Stout*, 1981; *Ishikawa et al.*, 2005]). This implies that the basal thrust acted as a main fluid pathway for fluids of variable compositions, over a broad range of pressure and temperature conditions over time. These protracted fluid-rock processes produced a complex suite of metasomatic sequences. Hereafter, we will focus on listvenitization and associated reactions and the respective contributions of the (metasomatized) protolith(s) and fluid compositions in the geochemical signature of the listvenite series.

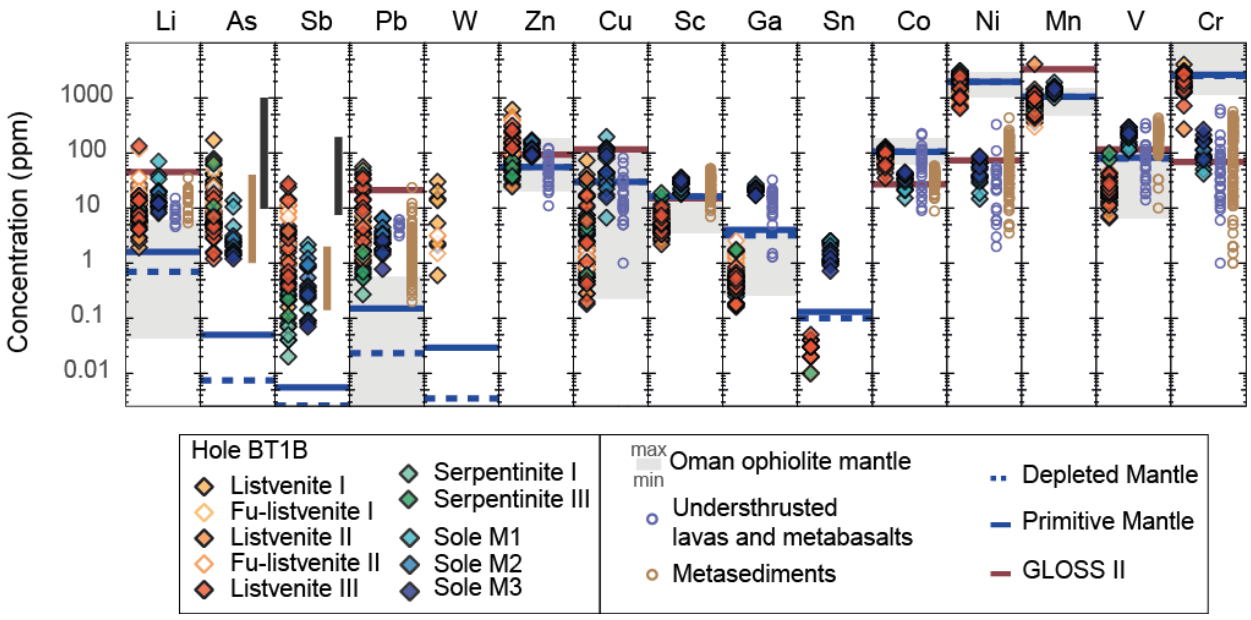


**Figure 7**. Caltech diagram of the composition of elemental abundance of BT1B listvenites series and metamorphic sole samples. Compositions are plotted on a log scale and compared with the compositional range of Oman ophiolite (grey field), primitive mantle [*McDonough and Sun*, 1995], depleted mantle [*Salters and Stracke*, 2004], the GLOSS II compilation of subducting sediments [*Plank*, 2014],and lavas and sediments from the metamorphic sole and the understhrusted Hawasina assemblages. As and Sb compositions are compared to the composition of abyssal plain sediments (brown line, [*Plank and Ludden*, 1992]) and hydrothermal sulfides (black line, [*Fouquet et al.*, 2010]). Literature data sources for the Oman Ophiolite, metamorphic sole and Hawasina assemblages are as in previous figures. Symbols are in inset.

The BT1B listvenites series are systematically enriched in FME, particularly Cs, Rb, Ba and K, relative to the Semail ophiolite mantle section (Fig. 6). These alkali-rich compositions typically characterize the basal Semail ophiolite mantle and its metamorphic sole; they are interpreted as evidence for interactions with slab derived aqueous fluids along the slab-mantle interface in both the metamorphic sole (e.g., [*Ambrose et al.*, 2021; *Ghent and Stout*, 1981; *Ishikawa et al.*, 2005]) and the adjacent mantle section, where it induces amphibole precipitation at the expense of clinopyroxene in basal lherzolites during incipient subduction (T > 600°; e.g., [*Khedr et al.*, 2013; *Khedr et al.*, 2014; *Prigent et al.*, 2018a; *Yoshikawa et al.*, 2015]) and serpentinization during ophiolite cooling (e.g., [*Lippard et al.*, 1986; *Prigent et al.*, 2018b]). The formation of these alkali-rich aqueous fluids is attributed to the de-volatilization in granulite-amphibolite facies conditions of the altered oceanic crust and associated sediments, with a potential contribution from the metamorphic sole (e.g., [*Prigent et al.*, 2018b]). The $CO_2$-rich fluids triggering the formation of listvenites probably derive from the same deep processes [*Kelemen et al.*, 2021]. Downhole variations in mineralogy and geochemistry, however, indicate a complex relationship between fluid ingress and reactions. This variation may relate to: (1) variable permeability along the core with respect to $CO_2$-rich fluids; (2) variable contributions of earlier fluid-rock interactions and late $CO_2$-metasomatism; (3) variation in the fluid composition, temporal and/or spatial; or any combination of the above. The latter of these could induce the

two observed reaction pathways: carbonation only in serpentinites and coupled carbonation/silicification reactions in listvenites.

The main mineralogical and petrophysical characteristics of the BT1B listvenite series are manifested in alternating bodies of variously carbonated serpentinite intervals with listvenites and fuchsite-bearing listvenites, a structural pattern also observed at the scale of the Wadi Mansah listvenite massif [*Falk and Kelemen*, 2015]. BT1B listvenites preserve textures indicating that they formed after serpentinites and, in spite of their strong differences in mineralogy and volatile element compositions, serpentinites and listvenites overlap in compositions for most major and trace elements, including alkali elements, suggesting that they both interacted with the same fluids (Figs. 4, 7). A recent clumped isotope thermometry study of BT1B listvenites indicates temperatures of listvenitization of 245-45°C [*Beinlich et al.*, 2020]). These temperatures are low compared to those anticipated for the serpentinization of the basal lherzolites by slab derived fluid (below 350°C) [*Prigent et al.*, 2018b] but there is a possible overlap. We propose that the ingress of $CO_2$-rich fluids occurred after the onset of serpentinization of basal lherzolites, and that the preservation of serpentinites indicates that flow paths were highly localized (likely fractures and veins). We cannot preclude however that serpentinization and the onset of listvenite formation were contemporaneous, with a possible contribution of the water released by listvenitization to the serpentinization of neighboring peridotites.

The main differences in the distribution of alkali elements, K, Ba, Cs and Rb, along the listvenite series are their selective enrichments in Listvenite domain II compared to Listvenite domains I and III. These enrichments are particularly prominent in the fuchsite-bearing listvenites. They are associated also to relatively low $Fe^{3+}/Fe$, overlapping Semail ophiolite mantle values and evidences of iron loss in individual samples (though not at the scale of the entire borehole, see Section 5.1) suggesting that fluid-rock interactions occurred in relatively reduced conditions (Fig. 2). The protolith of Listvenite Domain II was lherzolitic and contained higher $Al_2O_3$ and likely higher concentrations in alkali elements due to the occurrence of amphibole, compared to neighboring refractory peridotites. We propose that as $CO_2$-rich fluids interacted with the base of the Semail ophiolite, the chemical components necessary for the precipitation of fuchsite ($(K,Na)(Al,Cr,Fe)_2(Si,Al)_3O_{10}(OH,F)_3$) were abundant only in the fertile peridotite end-members. This triggered a suite of metasomatic reactions different from those taking place in the refractory protoliths, in turn possibly changing the local redox conditions (buffering of local $fO_2$ by Fe trapping in the fuchsite structure).

In contrast, the development of dolomite-dominated Ca and Sr rich intervals in Listvenite Domains I and III cannot be interpreted as solely resulting from changes in the protolith composition. The Ca-Sr rich intervals are located within and at the transition of (talc-bearing) serpentinites and listvenites, in the fractured upper part of Listvenite Domains I (48 to 53 mbg and 63 to 67 mbg) and throughout Listvenite Domain III, with Ca-Sr enrichments increasing toward the basal thrust. It is noteworthy that this downhole trend continues into the M1 metabasalts, drawing a shape similar to a diffusive front across the basal thrust (Fig. 2). Ca-Sr rich intervals also show increasing $Fe^{3+}/Fe_T$ values, in particular towards the basal thrust, systematically associated to the enrichments in (redox sensitive) U, suggesting fluid-rock interactions in an oxidized environment (e.g., [*Paulick et al.*, 2006; *Peters et al.*, 2017]). We interpret these compositions as resulting from interactions with Ca-, Sr and $CO_2$-rich fluids which sample a different source than the dominantly alkali-rich fluids driving listvenitization and

potentially earlier metasomatic processes documented along BT1B cores. Fluid pathways for these Ca-Sr-rich fluids were located mainly along the main lithological interfaces sampled at Hole BT1B; interactions with these fluids also overprinted the composition of the sole (M1 metabasalts). The change of source could be associated to a final stage of listvenitization associated with circulation of meteoric-derived fluids (e.g., New Caledonia [*Ulrich et al.*, 2014]) or evidence of an occasional change in the composition of the dehydrating slab at depth (carbonate reef capped seamounts as preserved by the Hawasina assemblages [*Lippard et al.*, 1986] or variable abundances of carbonate veins in altered oceanic crust [*Alt and Teagle*, 1999]). We favor the later interpretation as structural and lithological descriptions show that dolomitic matrix and veins are commonly crosscut by late magnesite and/or magnesite-quartz veins.

Selective and variable enrichments in other FME, such as Li, Pb, Sb and As or U (Figs. 2, 3 and 7) are observed along the core, sometimes in association to slight changes in Zn and Cu compositions or in $Fe^{3+}/Fe_T$. The most prominent occur at 18-35 mbg in the upper part of Listvenite domain I, and show enrichments in Li, Mn, U, Zn and Cu, and high $Fe^{3+}/Fe_T$, also independently of the presence of dolomite. This zone records extensive fracturing and re-cementation events, with locally the precipitation of oxides [*Menzel et al.*, 2020b]. These tectonic processes likely favored the development of localized fluid pathways and, in turn, more effective fluid-rock interactions and elemental redistributions along these domains.

These heterogeneous chemical distributions along the core indicate that solute transport was mainly advective into highly localized fluid pathways, likely in relation with the ubiquitous brittle and cataclastic fracturation that characterize the listvenite series. We posit that these reactive, mechanical and hydrodynamic processes were coupled at the local scale thus explaining the differences in calculated mass and volume changes along the core, resulting in the multiscale and high density network of crosscutting veins charactering the BT1B listvenite series [*Kelemen et al.*, 2021; *Kelemen et al.*, 2020b; *Menzel et al.*, 2020b]. The complex structure and mineralogy characterizing the listvenite series reflects a suite of metasomatic reactions forming overlapping reaction zones and triggered by interactions with fluids derived from (at least) two sources. The development of this metasomatic sequence depends on several thermodynamic (temperature, pressure), hydrodynamic (permeability, solute transport…) and chemical parameters (composition of the fluid and rock, redox…) that will vary with local tectonics (cooling, fracturing, …) and with the progress of the reactions (e.g., negative feedbacks between permeability and carbonation reactions [*Peuble et al.*, 2019; *Peuble et al.*, 2015]). In this context, determining the parameters controlling the sequence of fluid-rock reactions and the associated elemental redistribution is challenging. It requires an integrated petro-structural, mineralogical and in situ geochemical and isotopic investigation of the cores that is beyond the scope of this study.

### 5.3 Contribution of listvenites to global chemical budgets

Numerous studies have demonstrated the important contribution of (de-)serpentinization reactions to the deep Earth geochemical cycles of water and many fluid mobile elements (e.g., [*Deschamps et al.*, 2013; *Deschamps et al.*, 2011; *Kodolanyi et al.*, 2012; *Spandler and Pirard*, 2013]). Recent work has also shown the potential importance for the global carbon cycle of carbonation reactions affecting peridotites, from oceanic to subduction environments (e.g., [*Cannaò et al.*, 2020; *Kelemen and Manning*, 2015]). However, the possible consequences of peridotite carbonation, and in particular listvenitization, for the cycles of other chemical elements

is still little explored despite the fairly ubiquitous occurrence of listvenites in peridotite bodies and subduction-related ophiolites globally. Our study provides one of the first insights on these processes.

The BT1B listvenites are characterized by a dual geochemical signature: they preserve the composition(s) of their serpentinized protolith(s) for major elements (except for Ca) and most compatible (e.g., V, Sc, Ni, Cr, Co) and incompatible lithophile elements (e.g., REE, HFSE) (Fig. 6) yet, for fluid mobile elements, and in particular alkali elements (Li, K, Cs, Rb, K, Ba, Sr), Pb, As, Sb, and W, they have marked enrichments, with abundance similar or even enriched relative to metabasalts and metasediments such as those composing the metamorphic sole (Fig. 4, 6, 7). These FME enrichments are comparable to, though towards the upper end of the range of, those observed in most subduction related serpentinites (e.g., [*Deschamps et al.*, 2013; *Peters et al.*, 2017]) and ophicarbonates [*Cannao et al.*, 2020] where, as proposed for the Semail ophiolite-sole transition, they are attributed to interactions with fluids derived from de-volatilization reactions at depths of subducted sedimentary sequences or previously metasomatized altered oceanic lithosphere (Fig. 8). These compositions however differ from that of the serpentinites and ophicarbonates formed in oceanic environments (e.g., [*Cannao et al.*, 2020; *Noel et al.*, 2018; *Peters et al.*, 2017]), that all show significant U enrichments and, when carbonation occurs, selective enrichments in Ca and Sr, and in LREE, a trend observed in the BT1B variously carbonated serpentinites. The remobilization (Zn, Cu) and enrichments (As, Sb, Pb) of chalcophile elements and of selected siderophile elements (variable Ni, Co and Cr, and enrichments in W) is a common characteristic of listvenites that typically show ore-grade compositions for these elements (e.g., [*Belogub et al.*, 2017; *Buisson and Leblanc*, 1985; *Escayola et al.*, 2009; *Halls and Zhao*, 1995; *Laznicka*, 2010]). It should be noted that it is not solely related to subduction environments: such variations in compositions are observed also in highly serpentinized ultramafic basement of high temperature oceanic hydrothermal vents (e.g., [*Andreani et al.*, 2014]). However, rather than differences in the tectonic setting, these variable behavior in FME most likely reveal local changes in the conditions at which serpentinization and carbonation reactions occur. The precipitation of Ca-bearing LREE-rich hydrothermal carbonates and the mobility of U are favored in alkaline (serpentinization-derived) fluids at low temperature oxidizing hydrothermal conditions (e.g., [*Noel et al.*, 2018; *Paulick et al.*, 2006; *Seyfried Jr. et al.*, 1998]). In contrast, the remobilization of chalcophile and siderophile elements is commonly associated to interactions with high temperature saline hydrothermal fluids occurring over a broad range of redox conditions that will favor selective enrichments in serpentine (e.g., adsorption of As and Sb at oxidizing conditions) and the development of different suites of sulfides, oxides and/or metals depending on local redox (e.g., [*Andreani et al.*, 2014; *Belogub et al.*, 2017; *Cannao et al.*, 2020; *Fouquet et al.*, 2013; *Paulick et al.*, 2006]). As previously discussed, these variations in serpentinization and carbonation conditions depend first the distribution of fluid pathways, the timing of their formation, mostly in relation to the localization of deformation during cooling (e.g., [*Menzel et al.*, 2020b]). In turn, serpentinization and carbonation reactions modify the local chemical conditions by changing the mineralogy of the reacted samples and fluid composition (pH, alkalinity, ionic strength; e.g., [*Andreani et al.*, 2009; *Godard et al.*, 2013; *Grozeva et al.*, 2017; *Janecky and Seyfried*, 1986; *Peuble et al.*, 2019; *Peuble et al.*, 2015; *Seyfried et al.*, 2007]). As noted by Frost [1985]), they could lead in particular to extreme redox gradients as oxygen fugacity is buffered by the Fe-magnesite-Fe-oxide assemblage, and thus can attain values above those of the hematite-magnetite buffer in

magnesite-bearing listvenites compared to neighboring serpentinites, which in turn will likely impact the local sulfur speciation.

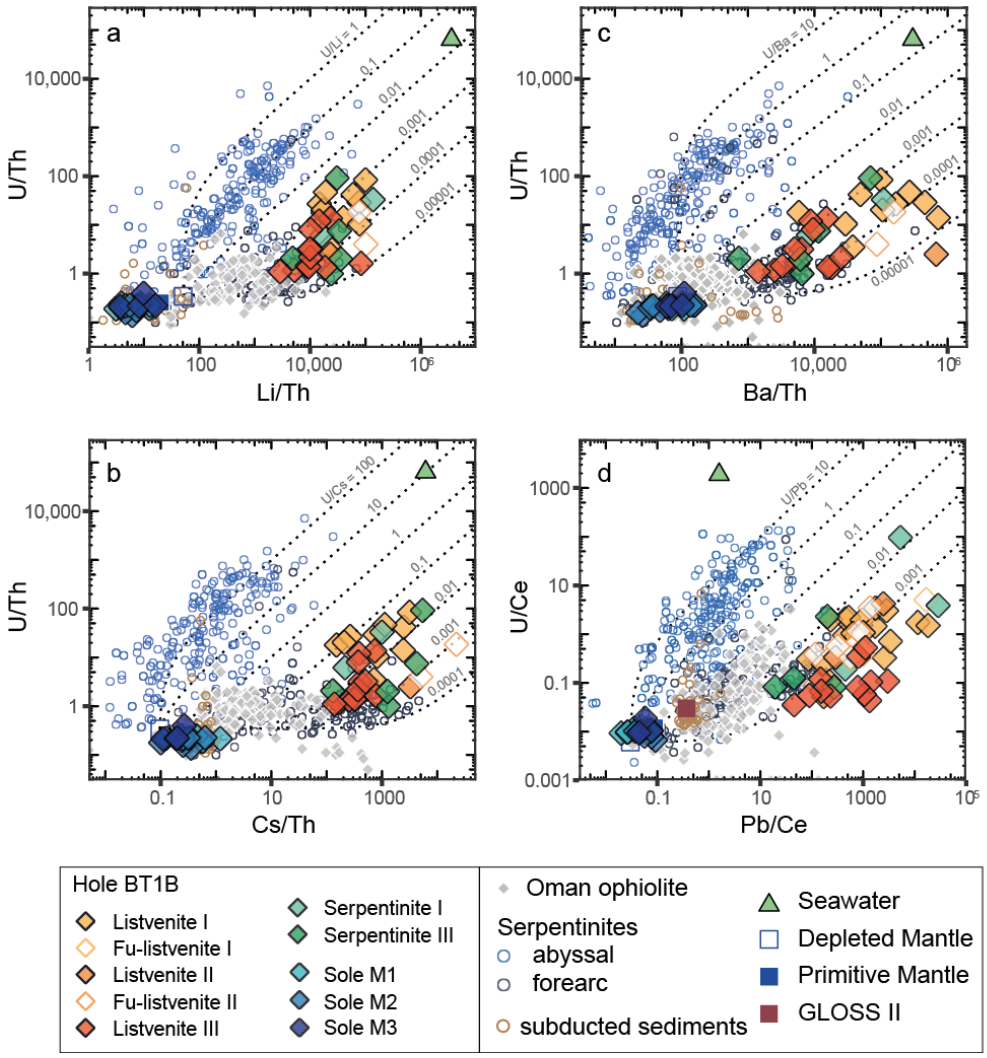


**Figure 8**. Scatterplots showing fluid mobile element enrichment relative to immobile trace elements in BT1B listvenites and serpentinites (a) U/Th versus Li/Th. (b) U/Th versus Cs/Th. (c) U/Th versus Ba/Th. (d) U/Ce versus Pb/Ce. Plotted for comparison are: compiled serpentinite compositions from abyssal (blue circles) and forearc (dark blue circles) settings (data from compilations in *Peters et al.* [2017] and *Deschamps et al.* [2013]); compiled Oman ophiolite data, sediments [*Plank et al.*, 2007], as well as the compositions of primitive mantle [*McDonough and Sun*, 1995], depleted mantle [*Salters and Stracke*, 2004], GLOSS-II [*Plank*, 2014] and seawater [*Li*, 1991]. Also plotted are lines of addition of fluid mobile elements in various ratios at fixed Th or Ce. Literature data sources for Oman ophiolite are as in previous plots. Symbols are in inset.

This complex suite of thermodynamic and chemical processes coupled to fluid fluxes, likely occurring far from equilibrium, explains the strong heterogeneity of geochemistry observed along the BT1B core and likely the disequilibrium textures characterizing most

carbonate-quartz assemblages in BT1B listvenites (e.g., [*Beinlich et al.*, 2020]). In particular, fast growth of magnesite could efficiently trap FME in fluid inclusions (e.g., [*Cannaò and Malaspina*, 2018]) and in microphases (e.g., sulfides), thus inducing their extreme elemental enrichments when compared to previously analyzed serpentinites and ophicarbonates (e.g., [*Cannao et al.*, 2020; *Deschamps et al.*, 2013; *Peters et al.*, 2017; *Spandler and Pirard*, 2013]). The same reactive transport mechanisms likely explains the preservation of the mantle signature by listvenites. The quartz forming silicification reactions observed throughout the core are not related to interactions with incoming fluids having high silica activity, as suggested for the formation of some listvenite bodies (e.g., [*Nasir et al.*, 2007; *Ulrich et al.*, 2014]). Local silica enrichments are most likely due to its incomplete removal during coupled silicate dissolution – carbonate precipitation reactions, a process commonly observed during reactive percolation hydrothermal experiments when carbonation kinetics are fast compared to solute transport (low fluid renewal at the surface of reacting minerals and/or slow diffusivity of solutes [*Peuble et al.*, 2019; *Peuble et al.*, 2015]).

The dichotomy in the signatures of the listvenite series lead to extreme fractionation between fluid mobile elements and immobile incompatible elements (e.g., Th or Ce), in particular for alkali elements (Li, Ba, Cs, Rb) and chalcophile elements (Pb) as illustrated on Fig. 8 with Li/Th of 2000-$10^5$, Ba/Th of 500-$10^6$, Cs/Th of 100-5000 and Pb/Ce up to $5x10^5$. Relative enrichments in U are comparatively less prominent with U/Th of 1-100 and U/Ce of 0.05-100. These values are however significantly higher than that of the possible sources of fluids such as the metamorphic sole and associated metasediments (e.g. Li/Th <30, Ba/Th<200, Cs/Th<20, U/Th<0.5, U/Ce<0.05 and Pb/Ce<0.5 for the metamorphic sole (this study) and GLOSS II [*Plank*, 2014]). These elemental fractionations follow trends similar to what observed for fore-arc serpentinites when compared to oceanic serpentinites [*Peters et al.*, 2017] but the degree of fractionation measured in the BT1B listvenite series is significantly higher. If recycled, these extreme compositions could affect that of the subduction-related volcanics (e.g., by inducing a prominent alkali-rich sedimentary signature) or, over longer time scales, the mantle isotopic signature, for instance for lead isotopes, due to their high Pb concentrations compared to U and Th (e.g., U/Pb <0.005). They could contribute to the development of a high Pb/Ce, low Th/Pb and U/Pb reservoir and be considered as a potential solution to the "first lead paradox" [*Hofmann*, 2008].

Further investigations are however required to assess the possible role of listvenitization reactions as an efficient elemental trap, and its contribution in global geochemical cycles. It should be noted that the formation of large listvenite massifs as drilled in Wadi Mansah is quite rare and that most listvenite bodies are embedded into serpentinite mélange (e.g., [*Nasir et al.*, 2007]). The change in rheology (from ductile serpentinite-talc to brittle quartz-dominated assemblages) associated to large and probably fast increases in mass and volume associated to listvenitization probably favor fracturation and mechanical erosion of the listvenite assemblages to accommodate volume changes. Such mechanisms would facilitate the entrainment downward along the subduction zone of listvenites within serpentinite mélanges.

## 6 Conclusions

During ICDP Oman Drilling Project, the transition from the base of the Semail ophiolite to the underlying metamorphic sole was drilled at Hole BT1B (Wadi Mansah). We analyzed the bulk major, volatile and trace element compositions of 65 variously carbonated peridotites

serpentinites and (fuchsite-bearing) listvenites, and 19 metamorphic rocks collected from recovered cores, with the aim to better constrain chemical transfers associated to peridotite carbonation along the ophiolite basal thrust.

The listvenite series record the formation of listvenites after a serpentinized peridotite protolith: this process is marked by $CO_2$ addition and $H_2O$ removal. Their bulk geochemistry is highly variable at the meter scale yet, on average, it is close to that of the refractory peridotites of the Semail mantle section for most major and lithophile trace elements, except of the fuchsite-bearing listvenite domain that has compositions overlapping that of the more fertile, often amphibole-bearing, basal lherzolites. This suggests preservation of the peridotite protolith geochemistry in spite of extensive peridotite carbonation. All samples are however enriched in fluid mobile elements compared to the composition of the Semail peridotites (up to ~$10^3$-$10^4$ x PM). They have concentrations similar to the metamorphic sole and/or associated metasediments for elements such as Cs, Sr and Ca and sometimes even higher for elements such as Pb, Li, As, and Sb. We also observe a decoupling between Sr-Ca enrichments and for other FME, indicating interactions with several batches of $CO_2$-rich fluids originating in neighboring lithologies or deeper along the basal thrust. These results suggest that peridotite carbonation could represent one of the major trap-and-release mechanisms for water and FME along convergent margins.

## Acknowledgments, Samples, and Data

This work benefited from fruitful discussions with Francoise Boudier, Cécile Prigent, Manuel Menzel and Emilien Oliot. The authors thank Céline Martin and Léa Causse for their assistance for trace element analyses at the Géosciences Montpellier clean lab facility and on the AETE-ISO platform ("Analyses des Eléments en Trace dans l'Environnement et ISOtopes"; OREME observatory, University of Montpellier).

This research used samples and/or data provided by the Oman Drilling Project. The Oman Drilling Project (OmanDP) has been possible through co-mingled funds from the International Continental Scientific Drilling Project (ICDP; Kelemen, Matter, Teagle Lead PIs), the Sloan Foundation – Deep Carbon Observatory (Grant 2014-3-01, Kelemen PI), the National Science Foundation (NSF-EAR-1516300, Kelemen lead PI), NASA – Astrobiology Institute (NNA15BB02A, Templeton PI), the German Research Foundation (DFG: KO 1723/21-1, Koepke PI), the Japanese Society for the Promotion of Science (JSPS no:16H06347, Michibayashi PI; and KAKENHI 16H02742, Takazawa PI), the European Research Council (Adv: no.669972; Jamveit PI), the Swiss National Science Foundation (SNF:20FI21_163073, Früh-Green PI), JAMSTEC, the TAMU-JR Science Operator, and contributions from the Sultanate of Oman Ministry of Regional Municipalities and Water Resources, the Oman Public Authority of Mining, Sultan Qaboos University, CNRS-Univ. Montpellier, Columbia University of New York, and the University of Southampton.

This study was funded by Project ANR-18-CE01-0014-01 LISZT.

Data will be available online on the Pangeae data archiving platform (https://www.pangaea.de/): the archiving of our data is in progress but the process is not complete. It is presently available as Supplementary Dataset S1.

## References


Agard, P., P. Yamato, M. Soret, C. Prigent, S. Guillot, A. Plunder, B. Dubacq, A. Chauvet, and P. Monié (2016), Plate interface rheological switches during subduction infancy: Control on slab penetration and metamorphic sole formation, *Earth and Planetary Science Letters*, *451*, 208-220, doi:https://doi.org/10.1016/j.epsl.2016.06.054.

Alt, J. C., and D. A. H. Teagle (1999), The uptake of carbon during alteration of ocean crust, *Geochim. Cosmochim. Acta*, *63*(10), 1527-1535.

Ambrose, T. K., D. J. Waters, M. P. Searle, P. Gopon, and J. B. Forshaw (2021), Burial, Accretion, and Exhumation of the Metamorphic Sole of the Oman-UAE Ophiolite, *Tectonics*, *40*(4), e2020TC006392, doi:https://doi.org/10.1029/2020TC006392.

Andreani, M., J. Escartin, A. Delacour, B. Ildefonse, M. Godard, J. Dyment, A. E. Fallick, and Y. Fouquet (2014), Tectonic structure, lithology and hydrothermal signature of the Rainbow massif (Mid-Atlantic Ridge 36°14'N), *Geochemistry, Geophysics, Geosystems*, *15*(9), 3543-3571, DOI: 3510.1002/2014GC005269.

Andreani, M., L. Luquot, P. Gouze, M. Godard, E. Hoise, and B. Gibert (2009), Experimental study of carbon sequestration reactions controlled by the percolation of $CO_2$ -rich brine through peridotites, *Environ. Sci. Technol.*, *43*(4), 1226-1231; DOI: 1210.1021/es8018429.

Azer, M. K., H. A. Gahlan, P. D. Asimow, H. S. Mubarak, and K. M. Al-Kahtany (2019), Multiple Stages of Carbonation and Element Redistribution during Formation of Ultramafic-Hosted Magnesite in Neoproterozoic Ophiolites of the Arabian-Nubian Shield, Egypt, *The Journal of Geology*, *127*(1), 81-107, doi:10.1086/700652.

Baumgartner, L. P., and S. N. Olsen (1995), A least-squares approach to mass transport calculations using the isocon method, *Economic Geology*, *90*(5), 1261-1270, doi:10.2113/gsecongeo.90.5.1261.

Bechennec, F., J. Le Metour, D. Rabu, C. Bourdillon-de-Grissac, P. de Wever, M. Beurrier, and M. Villey (1990), The Hawasina Nappes: stratigraphy, palaeogeography and structural evolution of a fragment of the south-Tethyan passive continental margin, *Geological Society, London, Special Publications*, *49*(1), 213-223, doi:10.1144/gsl.sp.1992.049.01.14.

Beinlich, A., O. Plümper, E. Boter, I. A. Müller, F. Kourim, M. Ziegler, Y. Harigane, R. Lafay, P. B. Kelemen, and t. O. D. P. S. Team (2020), Ultramafic Rock Carbonation: Constraints From Listvenite Core BT1B, Oman Drilling Project, *Journal of Geophysical Research: Solid Earth*, *125*(6), e2019JB019060, doi:https://doi.org/10.1029/2019JB019060.

Belgrano, T. M., L. W. Diamond, Y. Vogt, A. R. Biedermann, S. A. Gilgen, and K. Al-Tobi (2019), A revised map of volcanic units in the Oman ophiolite: insights intothe architecture of an oceanic proto-arc volcanic sequence, *Solid Earth*, *10*, 1181–1217, doi: 1110.5194/se-1110-1181-2019.

Belogub, E. V., I. Y. Melekestseva, K. A. Novoselov, M. V. Zabotina, G. A. Tret'yakov, V. V. Zaykov, and A. M. Yuminov (2017), Listvenite-related gold deposits of the South Urals (Russia): A review, *Ore Geology Reviews*, *85*, 247-270, doi:https://doi.org/10.1016/j.oregeorev.2016.11.008.

Boschi, C., A. Dini, L. Dallai, G. Ruggieri, and G. Gianelli (2009), Enhanced CO2-mineral sequestration by cyclic hydraulic fracturing and Si-rich fluid infiltration into serpentinites at Malentrata (Tuscany, Italy), *Chemical Geology*, *265*(1), 209-226, doi:https://doi.org/10.1016/j.chemgeo.2009.03.016.

Boskabadi, A., I. K. Pitcairn, M. I. Leybourne, D. A. H. Teagle, M. J. Cooper, H. Hadizadeh, R. Nasiri Bezenjani, and R. Monazzami Bagherzadeh (2020), Carbonation of ophiolitic ultramafic

rocks: Listvenite formation in the Late Cretaceous ophiolites of eastern Iran, *Lithos*, *352-353*, 105307, doi:https://doi.org/10.1016/j.lithos.2019.105307.

Boudier, F., A. Baronnet, and D. Mainprice (2010), Serpentine Mineral Replacements of Natural Olivine and their Seismic Implications: Oceanic Lizardite versus Subduction-Related Antigorite, *Journal of Petrology*, *51*(1-2), 495-512, doi:410.1093/petrology/egp1049, doi:10.1093/petrology/egp049.

Boudier, F., G. Ceuleneer, and A. Nicolas (1988), Shear zones, thrusts and related magmatism in the Oman Ophiolite; initiation of thrusting on an oceanic ridge, *Tectonophysics*, *151*(1-4), 275-296.

Boudier, F., and R. G. Coleman (1981), Cross section through the peridotite in the Samail ophiolite, southeastern Oman mountains, *J. Geophys. Res.*, *86*, 2573-2592.

Boudier, F., and A. Nicolas (1988), Special Issue: The ophiolites of Oman, *Tectonophysics*, *151*(1-4).

Boudier, F., and A. Nicolas (2018), Synchronous Seafloor Spreading and Subduction at the Paleo-Convergent Margin of Semail and Arabia, *Tectonics*, *37*(9), 2961-2982, doi:https://doi.org/10.1029/2018TC005099.

Buisson, G., and M. Leblanc (1985), Gold in carbonatized ultramafic rocks from ophiolite complexes, *Economic Geology*, *80*(7), 2028-2029, doi:10.2113/gsecongeo.80.7.2028.

Cannaò, E., and N. Malaspina (2018), From oceanic to continental subduction: Implications for the geochemical and redox evolution of the supra-subduction mantle, *Geosphere*, *14*(6), 2311-2336, doi:10.1130/ges01597.1.

Cannao, E., M. Scambelluri, G. E. Bebout, S. Agostini, T. Pettke, M. Godard, and L. Crispini (2020), Ophicarbonate evolution from seafloor to subduction and implications for deep-Earth C cycling, *Chem. Geol.*, *546*, 119626; doi:119610.111016/j.chemgeo.112020.119626, doi:10.1016/j.chemgeo.2020.119626.

Cannaò, E., M. Tiepolo, G. E. Bebout, and M. Scambelluri (2020), Into the deep and beyond: Carbon and nitrogen subduction recycling in secondary peridotites, *Earth and Planetary Science Letters*, *543*, 116328, doi:https://doi.org/10.1016/j.epsl.2020.116328.

Chauvet, F., H. Lapierre, R. C. Maury, D. Bosch, C. Basile, J. Cotten, P. Brunet, and S. Campillo (2011), Triassic alkaline magmatism of the Hawasina Nappes: Post-breakup melting of the Oman lithospheric mantle modified by the Permian Neotethyan Plume, *Lithos*, *122*(1), 122-136, doi:https://doi.org/10.1016/j.lithos.2010.12.006.

Coleman, R. G., and C. A. Hopson (1981), Oman ophiolite Special Issue, *J. Geophys. Res.*, *B86*(4), 2497-2782.

Cowan, R. J., M. P. Searle, and D. J. Waters (2014), Structure of the metamorphic sole to the Oman Ophiolite, Sumeini Window and Wadi Tayyin: implications for ophiolite obduction processes, *Geological Society, London, Special Publications*, *392*(1), 155-175, doi:10.1144/sp392.8.

Deer, W. A., R. A. Howie, and J. Zussman (1996), *An Introduction to the Rock-Forming Minerals (2nd Edition)*, 712 pp., Prentice Hall.

Deschamps, F., M. Godard, S. Guillot, and K. Hattori (2013), Geochemistry of subduction zones serpentinites: A review, *Lithos*, *178*("Serpentinites from mid-oceanic ridges to subduction", B. Reynard, M. Godard and S. Guillot, eds.), 96-127, doi:110.1016/j.lithos.2013.1005.1019.

Deschamps, F., S. Guillot, M. Godard, M. Andreani, and K. Hattori (2011), Serpentinites act as sponges for fluid-mobile elements in abyssal and subduction zone environments, *Terra Nova*, doi: 10.1111/j.1365-3121.2011.00995.x.

977 Dewandel, B. (2002), Structure et fonctionnement hydrogéologique d'un aquifère discontinu :
978 l'ophiolite d'Oman, Thèse de doctorat (Direction: F. Boudier) thesis, 328 p. pp, Montpellier 2,
979 Montpellier.
980 Ernewein, M., C. Pflumio, and H. Whitechurch (1988), The death of an accretion zone as
981 evidenced by the magmatic history of the Sumail ophiolite (Oman), *Tectonophysics*, *151*(Spec.
982 Issue - The ophiolites of Oman), 247-274.
983 Escayola, M. P., J. A. Proenza, C. R. Van Staal, N. Rogers, and T. Skulski (2009), The Point
984 Rousse listvenites, Baie Verte, Newfoundland: altered ultramafic rocks with potential for gold
985 mineralization in *Geol. Survey Report*, *09-1*, edited, pp. 1-12, Newfoundland and Labrador Dept
986 Natural Resources.
987 Falk, E. S., and P. B. Kelemen (2015), Geochemistry and petrology of listvenite in the Samail
988 ophiolite, Sultanate of Oman: Complete carbonation of peridotite during ophiolite emplacement,
989 *Geochimica et Cosmochimica Acta*, *160*, 70-90, doi:https://doi.org/10.1016/j.gca.2015.03.014.
990 Fouquet, Y., et al. (2010), Geodiversity of Hydrothermal Processes Along the Mid-Atlantic
991 Ridge and Ultramafic-Hosted Mineralization: a New Type Of Oceanic Cu-Zn-Co-Au
992 Volcanogenic Massive Sulfide Deposit, in *Diversity Of Hydrothermal Systems On Slow*
993 *Spreading Ocean Ridges*, edited, pp. 321-367, doi:https://doi.org/10.1029/2008GM000746.
994 Fouquet, Y., et al. (2013), Geodiversity of Hydrothermal Processes Along the Mid-Atlantic
995 Ridge and Ultramafic-Hosted Mineralization: a New Type Of Oceanic Cu-Zn-Co-Au
996 Volcanogenic Massive Sulfide Deposit, in *Diversity Of Hydrothermal Systems On Slow*
997 *Spreading Ocean Ridges*, edited by P. A. Rona, C. W. Devey, J. Dyment and B. J. Murton, pp.
998 321-367; doi:310.1029/2008gm000746, doi:10.1029/2008gm000746.
999 Frost, B. R. (1985), On the Stability of Sulfides, Oxides, and Native Metals in Serpentinite, *J.*
1000 *Petrol.*, *26*(1), 31-63; doi:10.1093/petrology/1026.1091.1031.
1001 Gerbert-Gaillard, L. (2002), Caractérisation géochimique des peridotites de l'ophiolite d'Oman :
1002 Processus magmatiques aux limites lithosphere/asthenosphere, Thèse de doctorat, Co-direction
1003 F. Boudier et M. Godard thesis, 266 pp, Montpellier 2, Montpellier.
1004 Ghent, E. D., and M. Z. Stout (1981), Metamorphism at the base of the Semail ophiolite,
1005 Southeastern Oman ophiolite, *J. Geophys. Res.*, *86*, 2557-2573.
1006 Glennie, K. W., M. G. A. Boeuf, M. W. Hugues Clark, M. Moody-Stuart, W. F. H. Pilaar, and B.
1007 M. Reinhardt (1974), *Geology of the Oman Mountains*, 423 pp., Neder. Mijn. Geol. Genoot.,
1008 Delft, Netherlands.
1009 Godard, M., D. Bosch, and F. Einaudi (2006), A MORB source for low Ti magmatism in the
1010 Semail ophiolite, *Chem. Geol.*, *234*, 58-78.
1011 Godard, M., J.-M. Dautria, and M. Perrin (2003), Geochemical variability of the Oman ophiolite
1012 lavas: Relationship with spatial distribution and paleomagnetic directions, *Geochem. Geophys.*
1013 *Geosyst.*, *4*(6), 8609, doi:8610.1029/2002GC000452.
1014 Godard, M., D. Jousselin, and J.-L. Bodinier (2000), Relationships between geochemistry and
1015 structure beneath a palaeo-spreading centre: A study of the mantle section in the Oman
1016 Ophiolite, *Earth Planet. Sci. Lett.*, *180*, 133-148.
1017 Godard, M., L. Luquot, M. Andreani, and P. Gouze (2013), Incipient hydration of mantle
1018 lithosphere at ridges: A reactive-percolation experiment, *Earth Planet. Sci. Lett.*, *371-372*, 92–
1019 102, doi: 110.1016/j.epsl.2013.1003.1052.
1020 Goodenough, K. M., M. T. Styles, D. Schofield, R. J. Thomas, Q. C. Crowley, R. M. Lilly, J.
1021 McKervey, D. Stephenson, and J. N. Carney (2010), Architecture of the Oman–UAE ophiolite:

evidence for a multi-phase magmatic history, *Arabian Journal of Geosciences*, *3*(4), 439-458, doi:10.1007/s12517-010-0177-3.

Grozeva, N. G., F. Klein, J. S. Seewald, and S. P. Sylva (2017), Experimental study of carbonate formation in oceanic peridotite, *Geochimica et Cosmochimica Acta*, *199*, 264-286, doi:https://doi.org/10.1016/j.gca.2016.10.052.

Halls, C., and R. Zhao (1995), Listvenite and related rocks: perspectives on terminology and mineralogy with reference to an occurrence at Cregganbaun, Co. Mayo, Republic of Ireland, *Mineralium Deposita*, *30*(3), 303-313, doi:10.1007/BF00196366.

Hanghoj, K., P. Kelemen, D. Hassler, and M. Godard (2010), Composition and genesis of depleted mantle peridotites from the Wadi Tayin massif, Oman ophiolite. Major and trace element geochemistry, and Os isotope and PGE systematics, *J. Petrol.*, *51*(1&2), 201-227, doi:210.1093/petrology/egp1077.

Hansen, L. D., G. M. Dipple, T. M. Gordon, and D. A. Kellett (2005), Carbonated serpentinite (Listwanite) at Atlin, British Columbia: A geological analogue to Carbon Dioxide sequestration, *The Canadian Mineralogist*, *43*(1), 225-239, doi:10.2113/gscanmin.43.1.225.

Hofmann, A. W. (2008), The enduring lead paradox, *Nature Geoscience*, *1*(12), 812-813, doi:10.1038/ngeo372.

Hopson, C. A., R. G. Coleman, R. T. Gregory, J. S. Pallister, and E. H. Bailey (1981), Geologic section through the Samail ophiolite and associated rocks along a Muscat-Ibra transect, southeastern Oman mountains, *J. Geophys. Res.*, *86*(Spc. Issue - Oman ophiolite), 2527-2544.

Ishikawa, T., S. Fujisawa, K. Nagaishi, and T. Masuda (2005), Trace element characteristics of the fluid liberated from amphibolite-facies slab: Inference from the metamorphic sole beneath the Oman ophiolite and implication for boninite genesis, *Earth Planet. Sci. Lett.*, *240*, 355-377.

Jamtveit, B., A. Malthe-Sørenssen, and O. Kostenko (2008), Reaction enhanced permeability during retrogressive metamorphism, *Earth and Planetary Science Letters*, *267*(3), 620-627, doi:https://doi.org/10.1016/j.epsl.2007.12.016.

Janecky, D. R., and W. E. Seyfried (1986), Hydrothermal serpentinization of peridotite within the oceanic-crust- Experimental investigations of mineralogy and major element chemistry, *Geochimica et Cosmochimica Acta*, *50*(7), 1357-1378, doi:10.1016/0016-7037(86)90311-x.

Kelemen, P., et al. (2021), Mass transfer into the leading edge of the mantle wedge: Initial Results from Oman Drilling Project Hole BT1B, *Earth and Space Science Open Archive*, https://doi.org/10.1002/essoar.10507370.10507371.

Kelemen, P. B., and C. E. Manning (2015), Reevaluating carbon fluxes in subduction zones, what goes down, mostly comes up, *Proceedings of the National Academy of Sciences*, *112*(30), E3997-E4006, doi:10.1073/pnas.1507889112.

Kelemen, P. B., J. Matter, E. E. Streit, J. F. Rudge, W. B. Curry, and J. Blusztajn (2011), Rates and Mechanisms of Mineral Carbonation in Peridotite: Natural Processes and Recipes for Enhanced, in situ CO2 Capture and Storage, in *Annual Review of Earth and Planetary Sciences, Vol 39*, edited by R. Jeanloz and K. H. Freeman, pp. 545-576, doi:10.1146/annurev-earth-092010-152509.

Kelemen, P. B., J. M. Matter, D. A. H. Teagle, J. A. Coggon, and the Oman Drilling Project Science Team (2020a), *Proceedings of the Oman Drilling Project*, College Station, TX.

Kelemen, P. B., J. M. Matter, D. A. H. Teagle, J. A. Coggon, and the Oman Drilling Project Science Team (2020b), Site BT1: fluid and mass exchange on a subduction zone plate boundary in *Proceedings of the Oman Drilling Project*, edited by P. B. Kelemen, J. M. Matter, D. A. H.

Teagle, J. A. Coggon and the Oman Drilling Project Science Team, International Ocean Discovery Program, College Station, TX.

Khedr, M. Z., S. Arai, and M. Python (2013), Petrology and chemistry of basal lherzolites above the metamorphic sole from Wadi Sarami central Oman ophiolite, *Journal of Mineralogical and Petrological Sciences*, *108*(1), 13-24, doi:10.2465/jmps.121026.

Khedr, M. Z., S. Arai, M. Python, and A. Tamura (2014), Chemical variations of abyssal peridotites in the central Oman ophiolite: Evidence of oceanic mantle heterogeneity, *Gondwana Research*, *25*(3), 1242-1262, doi:https://doi.org/10.1016/j.gr.2013.05.010.

Kodolanyi, J., T. Pettke, C. Spandler, B. S. Kamber, and K. Gmeling (2012), Geochemistry of Ocean Floor and Fore-arc Serpentinites: Constraints on the Ultramafic Input to Subduction Zones, *Journal of Petrology*, *53*(2), 235-270, doi:10.1093/petrology/egr058.

Lambart, S., H. M. Savage, B. G. Robinson, and P. B. Kelemen (2018), Experimental Investigation of the Pressure of Crystallization of Ca(OH)2: Implications for the Reactive Cracking Process, *Geochemistry, Geophysics, Geosystems*, *19*(9), 3448-3458, doi:https://doi.org/10.1029/2018GC007609.

Lapierre, H., A. Samper, D. Bosch, R. C. Maury, F. Béchennec, J. Cotten, A. Demant, P. Brunet, F. Keller, and J. Marcoux (2004), The Tethyan plume: geochemical diversity of Middle Permian basalts from the Oman rifted margin, *Lithos*, *74*(3), 167-198, doi:https://doi.org/10.1016/j.lithos.2004.02.006.

Laznicka, P. (2010), *Giant Metallic Deposits: Future Sources of Industrial Metals*, 949 pp., Springer.

Le Mée, L., J. Girardeau, and C. Monnier (2004), Mantle segmentation along the Oman ophiolite fossil mid-ocean ridge, *Nature*, *432*, 167-172.

Li, Y.-H. (1991), Distribution patterns of the elements in the ocean: A synthesis, *Geochimica et Cosmochimica Acta*, *55*(11), 3223-3240, doi:https://doi.org/10.1016/0016-7037(91)90485-N.

Linckens, J., M. Herwegh, and O. Müntener (2011), Linking temperature estimates and microstructures in deformed polymineralic mantle rocks, *Geochemistry, Geophysics, Geosystems*, *12*(8), doi:https://doi.org/10.1029/2011GC003536.

Lippard, S. J., A. W. Shelton, and I. G. Gass (Eds.) (1986), *The ophiolite of northern Oman*, 178 pp., Backwell Scientific Publications, London.

MacLeod, C. J., C. Johan Lissenberg, and L. E. Bibby (2013), "Moist MORB" axial magmatism in the Oman ophiolite: The evidence against a mid-ocean ridge origin, *Geology*, *41*(4), 459-462, doi:10.1130/g33904.1.

Maury, R. C., F. Béchennec, J. Cotten, M. Caroff, F. Cordey, and J. Marcoux (2003), Middle Permian plume-related magmatism of the Hawasina Nappes and the Arabian Platform: Implications on the evolution of the Neotethyan margin in Oman, *Tectonics*, *22*(6), 1073, doi:1010.1029/2002TC001483.

McDonough, W. F., and S. S. Sun (1995), The composition of the Earth, *Chem. Geol.*, *120*(3-4), 223-253.

Menzel, M. D., C. J. Garrido, and V. López Sánchez-Vizcaíno (2020a), Fluid-mediated carbon release from serpentinite-hosted carbonates during dehydration of antigorite-serpentinite in subduction zones, *Earth and Planetary Science Letters*, *531*, 115964, doi:https://doi.org/10.1016/j.epsl.2019.115964.

Menzel, M. D., C. J. Garrido, V. López Sánchez-Vizcaíno, C. Marchesi, K. Hidas, M. P. Escayola, and A. Delgado Huertas (2018), Carbonation of mantle peridotite by CO2-rich fluids:

the formation of listvenites in the Advocate ophiolite complex (Newfoundland, Canada), *Lithos*, *323*, 238-261, doi:https://doi.org/10.1016/j.lithos.2018.06.001.

Menzel, M. D., J. L. Urai, J. C. de Obeso, A. Kotowski, C. E. Manning, P. B. Kelemen, M. Kettermann, A. P. Jesus, Y. Harigane, and t. O. D. P. P. S. Team (2020b), Brittle Deformation of Carbonated Peridotite—Insights From Listvenites of the Samail Ophiolite (Oman Drilling Project Hole BT1B), *Journal of Geophysical Research: Solid Earth*, *125*(10), e2020JB020199, doi:https://doi.org/10.1029/2020JB020199.

Monnier, C., J. Girardeau, L. Le Mée, and M. Polvé (2006), Along-ridge petrological segmentation of the mantle in the Oman ophiolite, *Geochemistry, Geophysics, Geosystems*, *7*(11), doi:https://doi.org/10.1029/2006GC001320.

Nasir, S., A. R. Al Sayigh, A. Al Harthy, S. Al-Khirbash, O. Al-Jaaidi, A. Musllam, A. Al-Mishwat, and S. Al-Bu'saidi (2007), Mineralogical and geochemical characterization of listwaenite from the Semail Ophiolite, Oman, *Geochemistry*, *67*(3), 213-228, doi:https://doi.org/10.1016/j.chemer.2005.01.003.

Nicolas, A., F. Boudier, B. Ildefonse, and E. Ball (2000), Accretion of Oman ophiolite and United Emirates ophiolite. Discussion of a new structural map, *Marine Geophys. Res.*, *21*, 147-179.

Noel, J., M. Godard, E. Oliot, I. Martinez, M. Williams, F. Boudier, O. Rodriguez, C. Chaduteau, S. Escario, and P. Gouze (2018), Evidence of polygenetic carbon trapping in the Oman Ophiolite: petro-structural, geochemical, and carbon and oxygen isotope study of the Wadi Dima harzburgite-hosted carbonates (Wadi Tayin massif, Sultanate of Oman), *Lithos*, *323*(Special issue "Geological reactive systems from the mantle to the abyssal sub-seafloor", Godard, M., Fumagalli, P., Jamtveit, B., Menez., B., eds.), 218-237, doi:210.1016/j.lithos.2018.1008.1020.

Oberhänsli, R., A. S. Wendt, B. Goffé, and A. Michard (1999), Detrital chromites in metasediments of the East-Arabian continental margin in the Saih Hatat area: constraints for the palaeogeographic setting of the Hawasina and Semail basins (Oman Mountains), *International Journal of Earth Sciences*, *88*(1), 13-25, doi:10.1007/s005310050242.

Paulick, H., W. Bach, M. Godard, C.-J. Hoog, G. Suhr, and J. Harvey (2006), Geochemistry of abyssal peridotites (Mid-Atlantic Ridge, 15°20'N, ODP Leg 209): Implications for fluid/rock interaction in slow spreading environments, *Chem. Geol.*, *234*, 179-210.

Pearce, J. A., T. Alabaster, A. W. Shelton, and M. P. Searle (1981), The Oman ophiolite as a cretaceous arc-basin complex : evidence and implications, *Phil. Trans. R. Soc. Lond., A300*, 299-317.

Peters, D., A. Bretscher, T. John, M. Scambelluri, and T. Pettke (2017), Fluid-mobile elements in serpentinites: Constraints on serpentinisation environments and element cycling in subduction zones, *Chemical Geology*, *466*, 654-666, doi:https://doi.org/10.1016/j.chemgeo.2017.07.017.

Peters, T. J., A. Nicolas, and R. G. Coleman (Eds.) (1991), *Ophiolite genesis and evolution of the oceanic lithosphere*, 903 pp., Kluwer Academic Press, Dordrecht, Boston, London.

Peuble, S., M. Godard, P. Gouze, R. Leprovost, I. Martinez, and S. Shilobreeva (2019), Control of CO2 on flow and reaction paths in olivine-dominated basements: An experimental study, *Geochim. Cosmochim. Acta*, *252*, 16-38, doi:10.1016/j.gca.2019.1002.1007.

Peuble, S., M. Godard, L. Luquot, P. Gouze, and I. Martinez (2015), $CO_2$ geological storage in olivine rich basaltic aquifers: New Insights from flow-through experiments, *Applied Geochemistry*, *52*, 174-190; doi:110.1016/j.apgeochem.2014.1011.1024.

Plank, T. (2014), The Chemical Composition of Subducting Sediments, in *Treatise on Geochemistry (Second Edition)*, edited by H. D. Holland and K. K. Turekian, pp. 607-629, Elsevier, Oxford, doi:https://doi.org/10.1016/B978-0-08-095975-7.00319-3.

Plank, T., K. Kelley, R. Murray, and L. Q. Stern (2007), Chemical composition of sediments subducting at the Izu-Bonin trench, *Geochemistry, Geophysics, Geosystems, 8*(4), doi:https://doi.org/10.1029/2006GC001444.

Plank, T., and J. N. Ludden (1992), Geochemistry of sediments in the Argo Abyssal Plain at Site 765: A continental margin reference section for sediment recycling in subduction zone, in *Proceedings of Ocean Drilling Program, Scientific Results, vol. 123*, edited by F. M. Gradstein, J. N. Ludden and A. C. Adamson, pp. 167–189, doi: 110.2973/odp.proc.sr.2123.2158.1992, Ocean Drilling Program, College Station, Texas.

Power, I. M., A. L. Harrison, G. M. Dipple, S. A. Wilson, P. B. Kelemen, M. Hitch, and G. Southam (2013), Carbon Mineralization: From Natural Analogues to Engineered Systems, *Reviews in Mineralogy and Geochemistry*, *77*(1), 305-360, doi:10.2138/rmg.2013.77.9.

Prigent, C., P. Agard, S. Guillot, M. Godard, and B. Dubacq (2018a), Mantle wedge (de)formation during subduction infancy: evidence from the base of the Semail ophiolitic mantle, *J. Petrol.*, *59*(11), 2061-2091, doi:2010.1093/petrology/egy2090.

Prigent, C., S. Guillot, P. Agard, D. Lemarchand, M. Soret, and M. Ulrich (2018b), Transfer of subduction fluids into the deforming mantle wedge during nascent subduction: Evidence from trace elements and boron isotopes (Semail ophiolite, Oman), *Earth and Planetary Science Letters*, *484*, 213-228, doi:https://doi.org/10.1016/j.epsl.2017.12.008.

Reagan, M. K., et al. (2017), Subduction Initiation and Ophiolite Crust: New Insights From IODP Drilling, *International Geology Review*, 1-12; doi:10.1080/00206814.00202016.01276482.

Rioux, M., S. Bowring, P. Kelemen, S. Gordon, F. Dudás, and R. Miller (2012), Rapid crustal accretion and magma assimilation in the Oman-U.A.E. ophiolite: High precision U-Pb zircon geochronology of the gabbroic crust, *J. Geophys. Res.*, *117*(B07201), doi:10.1029/2012JB009273.

Rioux, M., J. Garber, A. Bauer, S. Bowring, M. Searle, P. Kelemen, and B. Hacker (2016), Synchronous formation of the metamorphic sole and igneous crust of the Semail ophiolite: New constraints on the tectonic evolution during ophiolite formation from high-precision U–Pb zircon geochronology, *Earth and Planetary Science Letters*, *451*, 185-195, doi:https://doi.org/10.1016/j.epsl.2016.06.051.

Rose, G. (1837), Mineralogisch-geognostiche Reise nach dem Ural, dem Altai und dem Kaspischen Meere, in *Reise nach dem nordlichen Ural und dem Altai - Volume 1*, edited by G. E. Reimer, Verlag der Sanderschen Buchhandlung, Berlin (Germany).

Salters, V. J. M., and A. Stracke (2004), Composition of the depleted mantle, *Geochemistry, Geophysics, Geosystems*, *5*(5), doi:https://doi.org/10.1029/2003GC000597.

Schroeder, T., W. Bach, N. Jöns, S. Jöns, P. Monien, and A. Klügel (2015), Fluid circulation and carbonate vein precipitation in the footwall of an oceanic core complex, Ocean Drilling Program Site 175, Mid-Atlantic Ridge, *Geochemistry, Geophysics, Geosystems*, *16*(10), 3716-3732, doi:https://doi.org/10.1002/2015GC006041.

Searle, M. P., and J. Cox (1999), Tectonic setting, origin, and obduction of the Oman ophiolite, *GSA Bulletin*, *111*(1), 104-122, doi:10.1130/0016-7606(1999)111<0104:tsoaoo>2.3.co;2.

Searle, M. P., and J. Malpas (1980), Structure and metamorphism of rocks beneath the Semail ophiolite of Oman and their significance in ophiolite obduction, *Transactions of the Royal Society of Edinburgh: Earth Sciences*, *71*(4), 247-262, doi:10.1017/S0263593300013614.

Searle, R. C. (2019), *Geology of the Oman Mountains, Eastern Arabia*, 478 pp., Springer, doi:10.1007/978-3-030-18453-7.

Seyfried Jr., W. E., X. Chen, and L. H. Chan (1998), Trace element mobility and lithium isotope exchange during hydrothermal alteration of seafloor weathered basalt: an experimental study at 350°C, 500 bars, *Geochim. Cosmochim. Acta*, *62*, 949-960.

Seyfried, W. E., D. I. Foustoukos, and Q. Fu (2007), Redox evolution and mass transfer during serpentinization: An experimental and theoretical study at 200 degrees C, 500 bar with implications for ultramafic-hosted hydrothermal systems at Mid-Ocean Ridges, *Geochimica et Cosmochimica Acta*, *71*(15), 3872-3886, doi:10.1016/j.gca.2007.05.015.

Soret, M., P. Agard, B. Dubacq, A. Plunder, and P. Yamato (2017), Petrological evidence for stepwise accretion of metamorphic soles during subduction infancy (Semail ophiolite, Oman and UAE), *Journal of Metamorphic Geology*, *35*(9), 1051-1080, doi:https://doi.org/10.1111/jmg.12267.

Spandler, C., and C. Pirard (2013), Element recycling from subducting slabs to arc crust: A review, *Lithos*, *170–171*, 208-223, doi:210.1016/j.lithos.2013.1002.1016.

Stanger, G. (1985), Silicified serpentinite in the Semail nappe of Oman, *Lithos*, *18*, 13-22, doi:https://doi.org/10.1016/0024-4937(85)90003-9.

Takazawa, E., T. Okayasu, and K. Satoh (2003), Geochemistry and origin of the basal lherzolites from the northern Oman ophiolite (northern Fizh block), *Geochem. Geophys. Geosyst.*, *4*(2), 1021, doi:1010.1029/2001GC000232.

Ulrich, M., M. Muñoz, S. Guillot, M. Cathelineau, C. Picard, B. Quesnel, P. Boulvais, and C. Couteau (2014), Dissolution–precipitation processes governing the carbonation and silicification of the serpentinite sole of the New Caledonia ophiolite, *Contributions to Mineralogy and Petrology*, *167*(1), 952, doi:10.1007/s00410-013-0952-8.

Ulven, O. I., B. Jamtveit, and A. Malthe-Sørenssen (2014), Reaction-driven fracturing of porous rock, *Journal of Geophysical Research: Solid Earth*, *119*(10), 7473-7486, doi:https://doi.org/10.1002/2014JB011102.

Villey, M., J. Le Metour, and X. De Gramont (1986), Geological map of Fanja, Sheet NF 40-3F. Explanatory Notes, BRGM and Oman Ministry of Petroleum & Minerals.

Warren, C. J., R. R. Parrish, D. J. Waters, and M. P. Searle (2005), Dating the geologic history of Oman's Semail ophiolite: insights from U-Pb geochronology, *Contrib. Mineral. Petrol.*, *150*(DOI 10.1007/s00410-005-0028-5), 403-422.

Wilde, A., L. Simpson, and S. Hanna (2002), Preliminary study of Cenozoic hydrothermal alteration and platinum deposition in the Oman Ophiolite, *Journal of the Virtual Explorer*, *6*, 7-13.

Wilson, A. (1960), The micro-determination of ferrous iron in silicate minerals by a volumetric and a colorimetric method, *Analyst*, *85*, 823–827.

Yoshikawa, M., M. Python, A. Tamura, S. Arai, E. Takazawa, T. Shibata, A. Ueda, and T. Sato (2015), Melt extraction and metasomatism recorded in basal peridotites above the metamorphic sole of the northern Fizh massif, Oman ophiolite, *Tectonophysics*, *650*, 53-64, doi:https://doi.org/10.1016/j.tecto.2014.12.004.

†**Oman Drilling Project Phase 1 Science Party**
Jürg Matter, University of Southampton, United Kingdom
Damon Teagle, University of Southampton, United Kingdom
Jude Coggon, University of Southampton, United Kingdom
Michelle Harris, Plymouth University, United Kingdom
Emma Bennett, Cardiff University, United Kingdom
Nico Bompard, University of Southampton, United Kingdom
Marine Boulanger, Centre de Recherches Pétrographiques et Géochimiques, France
Lyderic France, Université de Lorraine, France
Gretchen Früh-Green, ETH Zurich, Switzerland
Dieter Garbe-Schönberg, Christian-Albrecht University of Kiel, Germany
Benoit Ildefonse, Université de Montpellier, France
Ana Jesus, German University of Technology in Oman, Oman
Jürgen Koepke, Leibniz University Hannover, Germany
Louise Koornneef, Plymouth University, United Kingdom
Romain Lafay, University of Lausanne, Switzerland
Johan Lissenberg, Cardiff University, United Kingdom
Chris MacLeod, Cardiff University, United Kingdom
Dominik Mock, Leibniz University of Hanover, Germany
Tony Morris, Plymouth University, United Kingdom
Samuel Müller, Kiel University, Germany
Julie Noël, Université de Montpellier, France
Daniel Nothaft, University of Colorado, USA
Americus Perez, Kanazawa University, Japan
Philippe Pezard, Université de Montpellier, France
Nehal Warsi, AZD Engineering, Oman
David Zeko, University of British Columbia, Canada
Barbara Zihlmann, University of Southampton, United Kingdom
Mohamed-Amine Bechkit, Houari Boumedienne University, Algeria
Laurent Brun, University of Montpellier, France
Bernard Célérier, University of Montpellier, France
Gilles Henry, University of Montpellier, France
Jehanne Paris, University of Montpellier, France
Gérard Lods, University of Montpellier, France
Pascal Robert, Université de Lorraine, Nancy, France
Salim Al Amri, Ministry of Regional Municipalities and Water Resources, Sultanate of Oman
Mohsin Al Shukaili, Ministry of Regional Municipalities and Water Resource, Sultanate of Oman
Ali Al Qassabi, Ministry of Regional Municipalities and Water Resources, Sultanate of Oman
Kyaw Moe, Japan Agency for Marine-Earth Science and Technology (JAMSTEC), Japan
Yasu Yamada, Japan Agency for Marine-Earth Science and Technology (JAMSTEC), Japan
Eiichi Takazawa, Niigata University, Japan
Katsuyoshi Michibayashi, Shizuoka University, Japan
Natsue Abe, JAMSTEC, Japan
Tetsu Akitou, Okayama University, Japan
Salim Ahmed AlShahri, Public Authority for Mining, Oman
Hamood Hamed Shames Al-Siyabi, MRMWR, Oman
Saif Masoud Alhumaimi, Public Authority for Mining, Oman
Maqbool Hussein AlRawahi, MRMWR, Oman
Musaab Shaker Al Sarmi, Sultan Qaboos University, Oman
Bader Hamed Alwaeli, Sultan Qaboos University, Oman
Andreas Beinlich, Curtin University, Australia
Elliot Carter, University of Manchester, United Kingdom
Mike Cheadle, University of Wyoming, USA
Mark Cloos, University of Texas at Austin, USA
Matthew Cooper, University of Southampton, United Kingdom
Laura Crispini, University of Genova, Italy

Joëlle D'Andres (was Ducommun), Australian National University, Australia
Luke Deamer, Cardiff University, United Kingdom
Jeremy Deans, University of Southern Mississippi, USA
Kathi Faak, Ruhr-Universitaet Bochum, Germany
Rebecca Greenberger, California Institute of Technology, USA
Yumiko Harigane, National Institute of Advanced Industrial Science and Technology, Japan
Kohei Hatakeyama, Hiroshima University, Japan
Andrew Horst, Marshall University, USA
Takashi Hoshide, Akita University, Japan
Keisuke Ishii, Niigata University, Japan
Kevin Johnson, University of Hawaii, USA
Michael Kettermann, Aachen University, Germany
Hogyum Kim, Seoul National University, Republic of Korea
Jürgen Koepke, Leibniz University Hannover, Germany
Kentaro Kondo, Akita University, Japan
Alissa Kotowski, University of Texas at Austin, USA
Fatna Kourim, Academia Sinica, Taiwan
Yuki Kusano, Geological Survey of Japan, Japan
Catriona Menzies, University of Southampton, United Kingdom
Tomoaki Morishita, Kanazawa University, Japan
Tony Morris, Plymouth University, United Kingdom
Du Khac Nguyen, Kanazawa University, Japan
Toshio Nozaka, Okayama University, Japan
Keishi Okazaki, JAMSTEC, Japan
Suzanne Picazo, University of Lausanne, Switzerland
Ryoko Senda, Kyushu University, Japan
Yamato Tateishi, Okayama University, Japan
Jessica Till, University of Iceland, Iceland
Susumu Umino, Kanazawa University, Japan
Janos Urai, Aachen University, Germany
Yoichi Usui, JAMSTEC, Japan